Aquatic Toxicology 235 (2021) 105810

Contents lists available at ScienceDirect

Aquatic Toxicology

journal homepage: www.elsevier.com/locate/aqtox

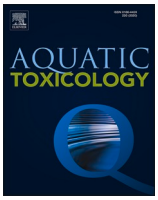

Low-level embryonic crude oil exposure disrupts ventricular ballooning and subsequent trabeculation in Pacific herring

John P. Incardona [a,*], Tiffany L. Linbo [a], Barbara L. French [a], James Cameron [b], Karen A. Peck [a], Cathy A. Laetz [a], Mary Beth Hicks [c], Greg Hutchinson [c], Sarah E. Allan [d], Daryle T. Boyd [a], Gina M. Ylitalo [a], Nathaniel L. Scholz [a]

[a] Northwest Fisheries Science Center, National Oceanic and Atmospheric Administration, Seattle, WA, USA
[b] Earth Resources Technology, under contract to Northwest Fisheries Science Center, National Oceanic and Atmospheric Administration, Seattle, WA, USA
[c] Oregon State University, Cooperative Institute for Marine Resources Studies, Hatfield Marine Science Center, Newport, OR, USA
[d] National Oceanic and Atmospheric Administration, Office of Response and Restoration, Anchorage, AK, USA

ARTICLE INFO

Keywords:
Forage fish
Cardiotoxicity
Heart development
Fish embryology
Polycyclic aromatic hydrocarbons
Cardiac hypertrophy
Oil spills

ABSTRACT

There is a growing awareness that transient, sublethal embryonic exposure to crude oils cause subtle but important forms of delayed toxicity in fish. While the precise mechanisms for this loss of individual fitness are not well understood, they involve the disruption of early cardiogenesis and a subsequent pathological remodeling of the heart much later in juveniles. This developmental cardiotoxicity is attributable, in turn, to the inhibitory actions of crude oil-derived mixtures of polycyclic aromatic compounds (PACs) on specific ion channels and other proteins that collectively drive the rhythmic contractions of heart muscle cells via excitation-contraction coupling. Here we exposed Pacific herring (*Clupea pallasi*) embryos to oiled gravel effluent yielding ΣPAC concentrations as low as ~ 1 μg/L (64 ng/g in tissues). Upon hatching in clean seawater, and following the depuration of tissue PACs (as evidenced by basal levels of *cyp1a* gene expression), the ventricles of larval herring hearts showed a concentration-dependent reduction in posterior growth (ballooning). This was followed weeks later in feeding larvae by abnormal trabeculation, or formation of the finger-like projections of interior spongy myocardium, and months later with hypertrophy (overgrowth) of the spongy myocardium in early juveniles. Given that heart muscle cell differentiation and migration are driven by Ca^{2+}-dependent intracellular signaling, the observed disruption of ventricular morphogenesis was likely a secondary (downstream) consequence of reduced calcium cycling and contractility in embryonic cardiomyocytes. We propose defective trabeculation as a promising phenotypic anchor for novel morphometric indicators of latent cardiac injury in oil-exposed herring, including an abnormal persistence of cardiac jelly in the ventricle wall and cardiomyocyte hyperproliferation. At a corresponding molecular level, quantitative expression assays in the present study also support biomarker roles for genes known to be involved in muscle contractility (*atp2a2, myl7, myh7*), cardiomyocyte precursor fate (*nkx2.5*) and ventricular trabeculation (*nrg2*, and *hbegfa*). Overall, our findings reinforce both proximal and indirect roles for dysregulated intracellular calcium cycling in the canonical fish early life stage crude oil toxicity syndrome. More work on Ca^{2+}-mediated cellular dynamics and transcription in developing cardiomyocytes is needed. Nevertheless, the highly specific actions of ΣPAC mixtures on the heart at low, parts-per-billion tissue concentrations directly contravene classical assumptions of baseline (i.e., non-specific) crude oil toxicity.

1. Introduction

As forage fish, Pacific herring (*Clupea pallasi*) are a keystone species for food webs in the northern Pacific Ocean and the Bering Sea (McKechnie et al., 2014). They spawn adhesive, demersal embryos on nearshore vegetation and other substrates and are therefore susceptible to developmental toxicity from shoreline pollution. This is particularly true for oil spills, including the 1989 Exxon Valdez and the 2007 Cosco Busan oil spills. These surface spills from grounded ships oiled the nursery habitats for herring shortly before the annual spawning seasons

* Corresponding author.
E-mail address: john.incardona@noaa.gov (J.P. Incardona).

https://doi.org/10.1016/j.aquatox.2021.105810
Received 2 December 2019; Received in revised form 18 February 2021; Accepted 16 March 2021
Available online 22 March 2021
0166-445X/

in Prince William Sound and San Francisco Bay, respectively. Following the Exxon Valdez spill, field collections of herring larvae that hatched along oiled shorelines identified an injury syndrome of developmental abnormalities typified most prominently by pericardial and yolk sac fluid accumulation (edema or "ascites"; Marty et al., 1997). Subsequent laboratory studies using an exposure system designed to emulate an oiled shoreline (effluent from oiled gravel columns) linked this syndrome to the bioconcentration of polycyclic aromatic hydrocarbons (PAHs), or more specifically, polycyclic aromatic compounds (PACs), a broader term that encompasses related heterocyclic compounds (Carls et al., 1999). The 2007 Cosco Busan bunker spill involved a different type of oil – namely, the bunker fuel used to power large marine vessels worldwide. Crude and bunker oils represent the beginning and end of the refinement process, respectively, and therefore have different chemical compositions (Uhler et al., 2007; Wang et al., 2003). Specifically, fuel oil is a residual and highly viscous fraction enriched in many contaminants with as-yet uncharacterized chemical and toxicological properties. The Cosco Busan oil proved highly lethal to herring embryos and larvae by a process involving photosensitization (Hatlen et al., 2010; Incardona et al., 2012b). This was in addition to the canonical cardiotoxic effects of PACs, which were evident as edema in caged (submerged) embryos and natural spawn up to two years after the spill (Incardona et al., 2012a).

For every fish species tested, embryonic exposure to crude oil leads to a syndrome of embryo-larval heart failure, marked by the accumulation of edema. This has been observed for an extensive diversity of freshwater and marine fish, exposure methods and geological sources of crude oil and its refinery fuel products (e.g., Adeyemo et al., 2015; Jung et al., 2017; Li et al., 2018; Linden, 1978; Madison et al., 2017; Pollino and Holdway, 2002; Raine et al., 2017). Studies over the past 15 years on Pacific herring and several other select species have identified specific aspects of cardiac failure as the central etiology of this crude oil developmental toxicity syndrome (reviewed by Incardona and Scholz, 2018; Incardona, 2017; Incardona and Scholz, 2016). Along a concentration-response gradient, exposures to petrogenic mixtures containing PACs at relatively high and yet environmentally-relevant levels (i.e., water concentrations of $\gtrsim$ 10 μg/L ∑PACs producing tissue levels of $\gtrsim$ 1000 ng/g wet weight) cause severe heart malformation, secondary extracardiac defects, and embryolarval lethality (e.g., Esbaugh et al., 2016; Incardona et al., 2009; Incardona et al., 2005; Incardona et al., 2004; Incardona et al., 2014; Jung et al., 2015; Morris et al., 2018; Sørhus et al., 2016b). At lower concentrations (i.e., $\lesssim$ 1 μg/L ∑PACs in water producing $\lesssim$ 200 ng/g wet weight in tissues), embryos survive transient cardiac dysfunction but subsequently grow poorly as juveniles with reduced survival rates (Heintz, 2007; Heintz et al., 2000; Incardona et al., 2015). Importantly, these survivors had subtle abnormalities in cardiac structure indicative of pathological remodeling, including altered ventricular shape, reduced compact myocardium, and hypertrophic spongy myocardium. These adverse anatomical changes were coupled in turn with reduced cardiorespiratory performance, as measured by lower critical swimming speeds (Hicken et al., 2011; Incardona et al., 2015). Consistent with these structural and functional abnormalities, transcriptome sequencing of isolated juvenile pink salmon (*Oncorhynchus gorbuscha)* hearts revealed changes in the expression of genes involved in cardiomyocyte proliferation and hypertrophy (enlargement or overgrowth), inflammation, and innate immunity (Gardner et al., 2019).

It is well established that cardiac function and form are inextricably interdependent processes that together shape heart development in fish and other vertebrates (for review see Andrés-Delgado and Mercader, 2016; Miquerol and Kelly, 2013). In this context, it has been shown that 3-ring classes of PACs that are commonly enriched in crude oil (e.g., the tricyclic phenanthrenes) directly and specifically interfere with cardiac function. This is evidenced by the disruption of cyclical action potential generation and intracellular calcium cycling in isolated heart muscle cells, or cardiomyocytes (Brette et al., 2014; Brette et al., 2017). These twin effects underlie the whole-heart phenotypes of 1) heart rate and rhythm defects and 2) reduced contractility observed in developing embryos (Edmunds et al., 2015; Incardona et al., 2009; Incardona et al., 2004; Incardona et al., 2014; Incardona et al., 2013; Jung et al., 2013; Morris et al., 2018; Sørhus et al., 2016b). Developmental genetics in zebrafish have clearly demonstrated a role for cardiac function in multiple aspects of late cardiogenesis, including chamber looping, initial proliferation of ventricular cardiomyocytes, outgrowth of the ventricule (ballooning) and formation of the internal spongy myocardium (trabeculation) (e.g., Berdougo et al., 2003; Dietrich et al., 2014; Jimenez-Amilburu et al., 2016; Rasouli and Stainier, 2017; Rottbauer et al., 2001); for a recent review, see (Sidhwani and Yelon, 2019). Intracellular Ca^{2+} handling is particularly central to many of these morphological processes, presumably via excitation-transcription coupling (reviewed by Ljubojevic and Bers, 2015; Wamhoff et al., 2006). Hypothesis-driven and exploratory transcriptome analyses of several marine fish embryos exposed to crude oil have identified changes in the expression of genes critical for cardiomyocyte Ca^{2+} dynamics, as well as transcription factors and signaling molecules with known roles in heart development (Edmunds et al., 2015; Sørhus et al., 2017; Sørhus et al., 2016b; Xu et al., 2016). At the upper end of the concentration-response relationship ($\gtrsim$ 10 μg/L ∑PACs), the crude oil cardiotoxicity syndrome mimics genetic loss-of-function in zebrafish (e.g., Arnaout et al., 2007; Ebert et al., 2005; Rottbauer et al., 2001), leading to complete heart failure and death soon after hatching (e.g., Esbaugh et al., 2016; Khursigara et al., 2017; Laurel et al., 2019). For wild fish that spawn in more lightly oiled habitats, uncertainty remains with respect to the mechanisms and processes that extend from mild functional impairment in transiently-exposed embryos to delayed toxicity in the form of altered cardiac structure and performance in surviving larvae, juveniles, or adults. Such latent impacts have been initially investigated in zebrafish (Hicken et al., 2011) as well as Pacific herring and pink salmon (Incardona et al., 2015).

Here we conducted a detailed anatomical and functional investigation of the hearts of Pacific herring through the larval and early juvenile stages following embryonic exposure to trace levels of crude oil. We specifically focused on circulatory-dependent morphogenetic processes that give rise to the fine structure of the developing ventricle, including the expression of genes known to be involved in the shape, orientation, and migration of ventricular cardiomyocytes during the major windows for initiation of ventricular ballooning and trabeculation). Lastly, we identify potentially novel molecular indicators at the embryonic stage that presage latent, abnormal cardiac remodeling in response to sublethal oil toxicity. These findings substantively refine and extend our current understanding of the PAC-driven adverse outcome pathway(s) in developing fish, and suggest new tools for measuring contaminant exposure and injury in the aftermath of future oil spills.

2. Materials and methods

2.1. Herring collection and fertilization

Ripe herring were captured from spawning aggregations by hook and line March 3, 2016 in Yaquina Bay, Newport, OR under Oregon Department of Fish and Wildlife permit #20039. Ovaries and testes were dissected and stored on ice in humidified 100 mm plastic Petri dishes until fertilization. The average mass of ovaries (mean ± S.D.) was 19.3 ± 5.2 g from 46 females with a fork length of 18.8 ± 1.0 cm and a total body mass of 81.4 ± 13.6 g. The corresponding weight of testes averaged 16.8 ± 5.3 g from 26 males with a fork length of 19.3 ± 1.0 cm and a total body mass of 81.0 ± 11.8 g. Fertilizations were carried out as detailed elsewhere (Griffin et al., 1998), using polyvinyl alcohol to prevent the clumping of eggs as they were distributed onto each of 16 sheets of 1 mm nylon mesh. Each 21×24 cm sheet held 10–20 g of embryos from 3–4 pooled females and two pooled males. Fertilizations were completed within a 3 hr period, and eggs were held overnight in a 4

ft tank supplied with 10ºC seawater. Subsequent microscopic assessment confirmed a successful fertilization rate of 76.2 ± 8.5%.

2.2. Exposure to oiled gravel effluents

Exposures were carried out at the NOAA Northwest Fisheries Science Center's Newport Research Station at the Hatfield Marine Science Center (Newport, OR) using filtered seawater pumped from adjacent Yaquina Bay maintained at 10ºC. Oiled gravel was prepared using artificially weathered Alaska North Slope crude oil as previously described (Incardona et al., 2012b). Gravel was coated with oil in a dosing series of 0.25, 0.5, and 1.0 g mass of oil per kg gravel. Columns were constructed using polyvinyl chloride plastic pipe (9.6 cm diameter) cut into 58 cm-tall sections and filled with ~ 1100 cm^3 of gravel. Water flow through each column (3.5 L/h) was vertical from an inflow at the base to an outflow at the top collected into individual 75-L glass aquaria fitted with outflow bulkheads to maintain a steady-state volume of ~ 68 L. A total of 16 columns were used, including n = 4 replicates of clean gravel (control treatment) and each of the three oil mass doses. Temperature in the exposure effluents was controlled by placing the aquaria in a water table supplied with high-flow, 10ºC seawater. The outflow from each aquarium was collected and decontaminated with activated charcoal. Embryos were exposed to column effluents beginning at 24 hr post-fertilization by vertically suspending the mesh sheets. Overall experimental design for exposure, transfer to clean water, post-exposure growth, all sample types and sampling points is provided in Fig. S1. Samples collected for lipid analyses were used to obtain dry weight values, but otherwise are the subject of a separate report.

2.3. Larviculture

Upon completion of the exposure window prior to hatching (10 dpf), each strip of remaining mesh with adhering embryos was cut into two equal pieces and transferred to the bottom of duplicate 400 L cylindrical flow-through fiberglass tank fitted with black plastic lining. Herring larvae hatched between 12 and 15 dpf. Hatching was quantified at 15 dpf by collecting 12 random images of each mesh and counting empty chorions and total embryos in each image. Total hatch per sheet was calculated as the mean percent empty chorions (N = 12), and the overall hatch per treatment calculated as the mean of the 4 sheets per dose. Clean seawater was supplied (1 - 5 L per min) through a submerged spray bar positioned at an angle near the bottom of the tank to minimize disturbance to the larvae. Additional water column circulation was provided by an air stone, and tanks were maintained at 10°C. Larvae were exposed to a light regimen consistent with ambient local conditions via skylight, supplemented by fluorescent lighting for 8:16 h light:dark. Larvae were fed live rotifers and brine shrimp. Rotifers (*Brachionus plicatilis*) were cultured in filtered and aerated seawater at 25-28°C, pH = 6.7-8.5, and a salinity 18-22 ppt adjusted using dechlorinated municipal freshwater. Brine shrimp (*Artemia*) were cultured in seawater with 0.75 g/L sodium bicarbonate at 25-30°C, pH = 8.0-8.5, salinity = 25-35 ppt, and a 2000 lux light intensity. Rotifers were enriched to 0.3 g/million for 8-16 hrs with Algamac (BioMarine) and *Artemia* were enriched to 0.5 g/L for 24 hrs with S.presso (Selco). Triplicate counts for either prey were determined daily via compound microscope, with feed volumes adjusted as needed to meet targeted densities.

Herring larvae were fed enriched rotifers from days 2-30 post-hatching at a density of 5 prey/ml (500,000 rotifers per 100 L seawater) twice daily. From days 5-124, larvae were fed enriched *Artemia* twice daily at a density of 2-4 prey/mL. To improve the visual contrast for larval capture of rotifer and shrimp prey, green water (Rotigrow Green, Reed Mariculture) was added to each grow-out tank prior to feeding. Beginning at 73 days post-hatch, herring larvae were transitioned to a custom trout feed (< 600 μm pellet size; Rangen) at a rate of twice daily. Individual tanks were cleaned weekly by siphoning.

2.4. Analysis of PACs in water and embryo tissues

Water samples (200 mL) were collected by glass pipet at exposure days 1 and 10, stabilized by the addition of 20 mL dichloromethane, and stored in glass amber bottles at 4ºC. At exposure day 10, ~ 1–2 g embryos were removed from each mesh, placed in pre-cleaned 125 mL glass I-CHEM jars (300 series; VWR Scientific), and stored at –20 ºC until analysis. Forty two PAC analytes were quantified (Data S1) as detailed previously (Sloan et al., 2014). In brief, samples were extracted with methylene chloride using separatory funnels (water) or an accelerated solvent extractor (tissue). PAC extracts were subsequently cleaned up by silica/aluminum columns (to remove highly polar compounds) and size-exclusion high-performance liquid chromatography (to remove lipids) before final quantification. The PACs were then separated on a 60 m DB-5 gas chromatography (GC) capillary column for detection on an electron impact mass spectrometer (MS) in selected-ion monitoring mode. In cases where a PAC compound was not detected in a sample, the value was reported as "less than the limit of quantification", or "<LOQ". A LOQ concentration was calculated for each sample based on sample mass and instrument performance for each batch of samples. Summed PAC concentrations (ΣPACs; see below) were calculated from detected values only. Complete PAC data are provided in supplemental file Data S1.

2.5. Sampling and live imaging of embryos and larvae

For gene expression analyses, embryos were sampled every other day during exposures (2, 4, 6, 8, and 10 dpf). A section was trimmed from each mesh and 20 embryos per exposure replicate (4 replicates per treatment) were removed after confirmation of viability via stereomicroscope inspection. After hatch (14 dpf), free-swimming yolk-sac larvae (20 per replicate) were randomly captured from the water column by wet bailing and concentration in cell strainers (Falcon 100 μm mesh, VWR #21008-950), anesthetized with MS-222, and transferred to sample collection tubes. Embryos and larvae were flash frozen on liquid nitrogen and stored at -80 ºC until extraction.

For phenotypic quantification after hatch, yolk sac larvae were randomly captured from each replicate tank, concentrated in cell strainers, and anesthetized with MS-222 titrated to inhibit a touch response. For each replicate, 30 larvae were mounted laterally (anterior to left) in 100-mm petri dishes filled with agarose containing slots molded into it by glass capillary tubes. Petri dishes were filled with seawater and maintained at 12 ºC using Peltier-cooled microscope stages (Brook Industries, Lake Villa, IL). Ten second digital video clips were collected for each larva focused on the heart region using the highest magnification on Nikon SMZ-800 stereomicroscopes fitted with Unibrain Fire-i780c cameras (Unibrain.com), connected via firewire to a laptop computer with the BTV Pro application (Bensoftware.com). For each replicate, several larvae were selected at random for representative composite images of the entire animal. Using two imaging stations, 480 larvae were imaged over an 8-hour period, with all dose levels randomized throughout. After imaging, larvae were collected into sample tubes (30 per tube) fixed for several hours in 4% Millinog's phosphate-buffered paraformaldehyde, rinsed in phosphate-buffered saline (PBS), and then transferred into methanol and stored at -20 ºC. Similar methods were used to capture digital images and video from and subsequently fix representative larvae for each treatment at 20 and 67 dpf. At 125 dpf, fish were sacrificed by MS-222 overdose and the hearts dissected in herring Ringer's solution, immediately digitally photographed in the lateral and dorsal views using Nikon SMZ-800s, and then fixed in Dietrich's solution overnight and stored in 70% ethanol at – 20ºC. Fork length (FL) and weight (W) were collected for each fish at 125 dpf, and these measures used to calculate the condition factor K, using the formula $K = FL\ (cm) / W(g)^3 \times 100$.

Table 1.
QPCR primers.

Gene	Forward primer	Reverse primer	NCBI Reference Sequence	Efficiency (%)
Reference genes				
ef1a	CTGGTATGGTTGTGACCTTCG	ACGGATATCCTTGACTGACACG	XM_012818387.1	105
mtm1	CTCTGAAGCAGGAGGGTCAC	CTGACTGAGGAACGCAAACA	XM_012817813.1	113
rxrba	ACCGATCTTCAGGCAAACAC	GGTACCTGAGCCATCGGTAA	XM_012833519.1	84
spop1	TTTCAGTGCGATGTTTGAGC	GCTTTCCCCGTGTAGATGAA	XM_012825971.1	101
wdtc1	GCTCTTCGCCAAGACAGATT	AGTTGTGGAAACGGATGGAG	XM_012838768.1	109
Target genes				
atp2	AGATCATCGAGTTCCTGCAGTC	CATGTTGTTGTAGATTGCCCGG	XM_012814918.1	112
cyp1a	AGGAGCACATCAGCAAGGAG	ACCACCTGTCCGAACTCATC	XM_012831254.1	110
hbegfa	TGGCAAACATCCGTAAACCTTC	TTTTCAACATCATAGGCACCCC	XM_012842112.1	100
nac2	TGTCATTGGCTTCCTCACTGC	CCCTGCACATTCCAGTAGATAGC	XM_012828862.1	120
nkx2.5	TGGATATTGTCAAGGAGGGGAAG	CTCGGGTGCAGACAAGTATTTCTG	XM_012831385.1	115
notch1	TGGAGCCAACAAAGACATGC	GCTAGGAACAGGGGAGTCTC	XM_012830546.1	117
myh7	AGGGCTCCTCTTTCCAAACT	AAGCCCTTTCTGCAGATCCT	XM_012827835.1	108
myl7	GAGGCTTTTGGTTGCATTGATC	TCATCCTTGTTGACGAATCCTG	XM_012831367.1	108
nrg2	TCGTCCACTCATGCCCATTC	CGGACACATACCTTTCACTGTG	XM_012821330.1	116
ryr2	GCTTGCTTGCAGTAGTGGTTTATC	GATGGCCAGCAGAATGACAATC	XM_012814530.1	137

2.7. Antibody labeling and imaging

For 67 dpf samples, whole herring larvae were rehydrated from storage in fixative via a graded methanol-PBS series. The trunk was then transected just posterior to the heart to facilitate whole mount immunolabeling. Head structures were subsequently permeabilized with distilled water (10 min) followed by several hours incubation in PBS + 0.1% Triton X-100 (PBT) with 3% normal goat serum. The tissues were then incubated overnight at room temperature in an anti-myosin heavy chain monoclonal antibody MF20 (Developmental Studies Hybridoma Bank, University of Iowa) at 1 μg/mL. After three PBT washes (several hours each), the samples were incubated overnight in AlexaFluor-568-conjugated goat-anti-mouse IgG_{2b} secondary antibody (ThermoFisher Scientific), cleared in 50% glycerol/PBS, and then labeled with 300 nM DAPI (20 min). Finally, whole hearts were carefully dissected from the head structures and mounted under a coverslip either laterally or ventral side up in 3% methylcellulose. Fluorescence was imaged using a Zeiss LSM5 Pascal confocal system with 405 and 543 nm laser excitation lines.

Hearts dissected from 125 dpf fish were embedded in paraffin and sectioned at 5 μm thickness. Slides were de-paraffinized in xylene substitute, hydrated through an alcohol series, and rinsed with dH_2O. Antigen unmasking was performed by heating tissue sections at 94 – 99°C in buffer containing 10 mM sodium citrate and 0.05% Tween 20, pH 6.0, for ten minutes, followed by cooling at room temperature for thirty minutes. In a room temperature humidity chamber, slides were treated for 5 min with PBS, then 30 min with block solution (PBS, 0.1% Triton X-100, 5% heat-inactivated normal goat serum, 1% DMSO, and 0.02% sodium azide), then overnight with primary antibody (anti-myosin heavy chain, MF20) at 1 μg/ml in block solution. This was followed by three washes for five minutes each with PBST (PBS and 0.1% Tween X-100), then overnight incubation with secondary antibody (goat anti-mouse IgG Alexa Fluor 488, ThermoFisher Scientific #A-11001) diluted 1:2,000 in block solution. Slides were then washed three times for five minutes each with PBST, and five minutes with PBS. Nuclei were stained with 600 nM DAPI (Invitrogen #D3571) in PBS for five minutes, followed by three rinses with PBS. Slides were mounted in 50% glycerol in PBS and 2-3 sections per heart (6 control, 7 exposed) imaged using an AxioCam HRm digital camera and a Zeiss LSM 5 Pascal confocal system with an Ar laser. Fiji software was used to quantify the number of DAPI+ nuclei and the percent trabeculation within the ventricle. Region Of Interest selection was used to measure total ventricle area and Color Threshold analysis was used to quantify percent MF20+ ROI within the entire ventricle (percent trabeculation). Sections for imaging were selected based on similar profiles of central structures (e.g., bulbus arteriosus and atrioventricular valve).

2.8. RNA extraction and quantitative real-time PCR

Total RNA was extracted by homogenizing samples in TRIzol (5% v/v, ThermoFisher Scientific) and then purified with a Direct-zol™ RNA MiniPrep column (Zymo Research Cat# R2051). RNA concentrations and purities were measured using a Nanodrop ND-1000 Spectrophotometer. Superscript IV (Thermofisher Cat #18090050) with oligo dt (20) primers was used to synthesize cDNA. For characterization of cardiac target genes, hearts and swimming muscle samples were collected from each of three 1-yr old cultured juvenile fish obtained from the US Geological Survey's Western Fisheries Research Center Marrowstone Field Station.

Reverse transcriptase quantitative polymerase chain reaction (qPCR) was performed on a Viia™ 7 Real-Time PCR system with Fast SYBR Green (ThermoFisher Scientific). Gene-specific RT-qPCR primers were designed using Primer3 (http://bioinfo.ut.ee/primer3/) and synthesized by Integrated DNA Technologies, Inc. (Coralville, Iowa). Herring-specific target sequences for primer design were identified by BLAST searches based on sequences from either an Atlantic haddock (*Melanogrammus aeglefinus*) embryonic transcriptome (Sørhus et al., 2016a; Sørhus et al., 2017) or the coding region of zebrafish genes (National Center for Biotechnology Information online database), using either an Atlantic herring (*C. harengus*) genome assembly (NCBI accession number ASM96633v1; (Martinez Barrio et al., 2016) or two published Pacific herring transcript libraries (Roberts et al., 2012). The herring genes identified by this approach were annotated using BLAST-based sequence alignments. Primer sequences are provided in Table 1.

Candidate reference genes were selected based on a lack of oil exposure treatment effect from the previously published Atlantic haddock embryonic and larval transcriptomes (Sørhus et al., 2017). These included *ef1a* (elongation factor 1 alpha), *mtm1* (myotubularin 1), *rxrba* (retinoid receptor X beta a), *spop1* (speckle type BTB/POZ protein 1), and *wdtc1* (WD and tetratricopeptide repeats 1). Absence of an oil exposure effect for herring orthologs of these genes was confirmed by analyzing qPCR data for the current herring oil exposure using a consensus of BestKeeper, GeNorm, and NormFinder algorithms with the RefFinder program (Xie et al., 2012). Based on this analysis, *mtm1* was eliminated and the other four genes retained (*ef1a, rxrba, spop1* and *wdtc1*). The reference gene selection approach was validated by running target gene qPCR raw data through the same algorithms, which failed in each case. Due to the low RNA yield of samples, primer efficiency was measured using standard curves generated from cDNA synthesized from the same cohort. Primer efficiencies and r^2 values were within acceptable range for each reference gene (Nolan et al., 2006). Normalized quantification threshold (Ct) values (dCt) and fold-change values relative to controls were calculated with the Comparative Ct method, using

Table 2.
PAC concentrations in water and Pacific herring embryo tissues.

Oil load	Water Day 1 (μg/L)	Water Day 10 (μg/L)	Tissue Day 10 (ng/g wet weight)	Tissue Day 10 (ng/g lipid)
Control	0.070 ±0.002	0.014 ± 0.003	10.2 ± 0.9	619 ± 99
0.25 g/kg	1.33 ± 0.13	0.26 ± 0.04	63.8 ± 10.3	3960 ± 723
0.5 g/kg	1.85 ± 0.17	0.72 ± 0.16	140.3 ± 35.9	8025 ± 2104
1.0 g/kg	4.15 ± 0.57	0.81 ± 0.02	237.5 ± 27.2	12879 ± 1486

the geometric mean of the four reference genes (Schmittgen and Livak, 2008).

2.9. Data analysis and statistics

Cardiac morphology and function were quantified from digital videos collected from yolk sac larvae at hatch (14 dpf). All video files were blinded and analyzed with ImageJ (https://imagej.nih.gov/ij/), with a consistent individual observer measuring all of the quantitative aspects of a given phenotype across replicates and treatments. Each video was carefully screened for quality criteria (e.g., alignment of specimen), and those not passing all criteria for a particular phenotype were excluded for that measure. Each endpoint was measured from a minimum of 23 larvae per replicate. Heart rates were measured by manually counting the number of complete contractions in each 10 sec video clip. The presence of edema was scored by deformation of the anterior yolk margin and increased pericardial area measured as detailed elsewhere (Incardona and Scholz, 2016). Heart chamber areas were measured with the freehand trace tool in ImageJ, at peak diastole and systole as identified by manually advancing through frames. Total areas for both chambers were measured at both phases of the cardiac cycle, while the posterior balloon portion of the ventricle was measured only at diastole. Cardiac jelly thickness was measured with the ImageJ straight line tool in the first 10 videos collected for each replicate, at the same location in the posterior ventricle and ventral wall of the atrium. Fractional shortening and AV angle were calculated from the chamber diameters as described elsewhere (Edmunds et al., 2015).

Data were analyzed by regression models using Prism 7 (GraphPad Software). Nonlinear models were used for cardiac endpoints, with specific (Edmunds et al., 2015) model parameters selected by statistical comparison. Lowest effective doses were determined by one-way ANOVA using JMP 13 (SAS Institute), with replicates nested within treatment to resolve tank effects. If a tank effect was present ($p \leq 0.05$), a one-way ANOVA was performed on replicate means. Means were compared using Dunnett's post-hoc test. Trabecular spacing data were analyzed by ANOVA with individual fish nested within treatment, followed by Dunnett's post-hoc test.

3. Results

3.1. Measured PAC concentrations in exposure water and herring tissue

As anticipated from previous oiled gravel column studies (e.g., Incardona et al., 2012b), PAC levels were in the target range for the nominal levels of gravel coating and declined over time (Table 2 and Data S1). The initial total (∑)PAC concentrations for the 0.25, 0.5 and 1.0 g/kg oiled gravel treatments (averaged across the four replicate columns) were 1.3 ± 0.1, 1.9 ± 0.2 and 4.2 ± 0.6 μg/L, with clean gravel controls at 0.070 ± 0.002 μg/L. The PAC compositions (Fig. S2) showed a fairly weathered pattern, dominated by naphthalene and phenanthrene homologs with higher degrees of alkylation (i.e., C3- and C4-naphthalenes and C2- and C3-phenanthrenes). By the end of exposure (day 10), embryos accumulated 64 ± 10, 140 ± 36, and 238 ± 27 ng/g ∑PACs for the 0.25, 0.5 and 1.0 g/kg oiled gravel columns, respectively, with control tissue concentrations at background levels of 10 ± 1 ng/g. When corrected for embryo lipid content (Table 2), this dosing range (∑PAC ~ 4000 – 13,000 ng/g lipid) overlaps closely with previous pink salmon exposures (~ 2000 – 23,000 ng/g lipid) yielding oil-induced abnormalities in juvenile heart function, histological structure, and gene expression (Gardner et al., 2019; Incardona et al., 2015). For the low and medium column loading treatments (0.25 and 0.5 g/kg oil/gravel), the PAC patterns were shifted slightly toward a higher ratio of phenanthrenes to naphthalenes in both water and tissue (Fig. S2B and C). Overall, tissues showed proportionally higher levels of phenanthrenes compared to naphthalenes, in relation to the respective levels in water (e.g., Fig. S2D top/bottom).

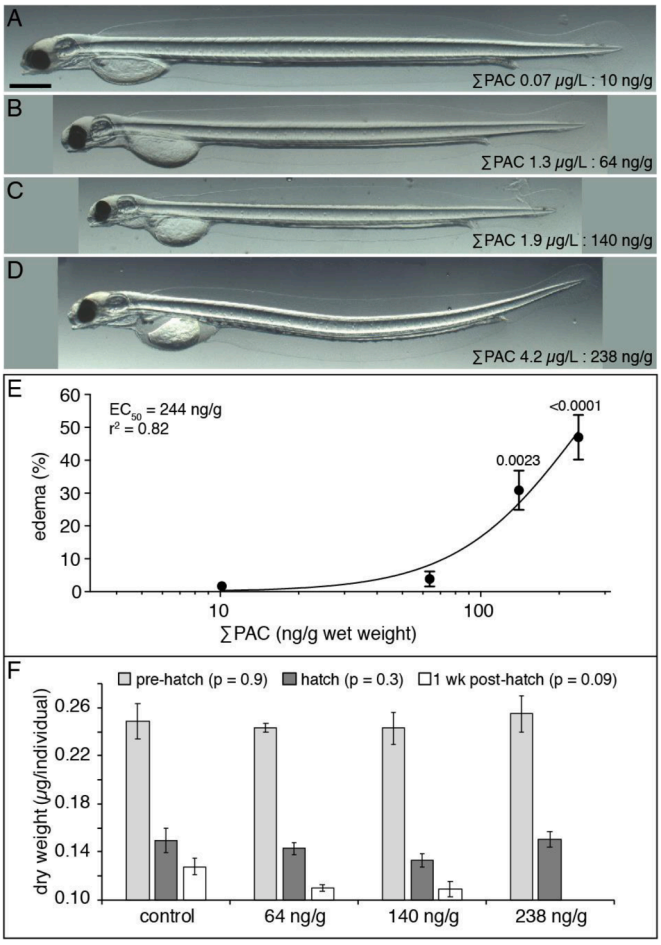

Fig. 1. Effects of embryonic exposure on gross morphology of yolk sac larvae. (A – D) Representative images of yolk sac larvae at peak hatch. (A) control; (B) 64 ng/g (1.3 μg/L) dose; (C) 140 ng/g (1.9 μg/L) dose; (D) 238 ng/g (4.2 μg/L) dose. Scale bar (A) is 1 mm. (E) Relationship between tissue dose and incidence of pericardial edema scored as deformation of the anterior yolk mass. Data are mean ± s.e.m. (N = 4) for 30 larvae from each of 4 replicate exposures per dose. (F) Dry weights of embryos at end exposure (light gray bars) and larvae at hatch (dark gray bars) and 1-week post-hatch (white bars). Data are mean ± s.e.m. (N = 4) for each of 4 replicate pools of 50 embryos or larvae, normalized per individual.

3.2. Induction of cyp1a mRNA

To further characterize PAC uptake we examined the expression of mRNA encoding cytochrome P4501A (CYP1A), the primary PAC-metabolizing enzyme that is induced following PAC binding to the

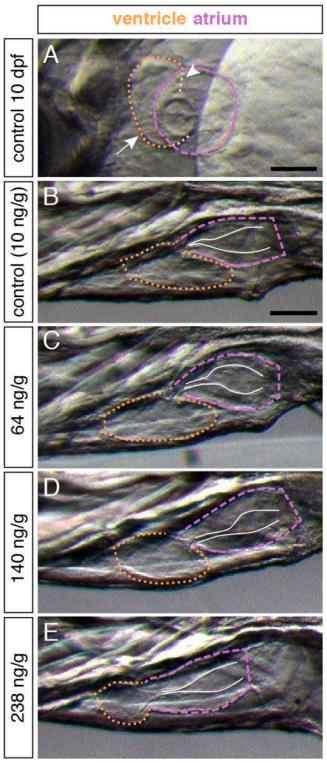

Fig. 2. Dose-dependent reduction in the degree of ventricular ballooning at hatch. High magnification lateral views of the heart are shown with anterior to the left, representing video frames taken from the end of ventricular diastole/atrial systole. The atrium is outlined by the dashed light magenta line, ventricle outlined by the orange dotted line. The solid white line traces the atrial endocardium. (A) 10 dpf control embryo, with white arrow indicting the ventricle outer curvature and white arrowhead indicating the inner curvature (behind atrium). Hatched yolk sac larvae shown for control (B), 64 ng/g dose (C), 140 ng/g dose (D) and 238 ng/g dose (E). Scale bar is 50 μm.

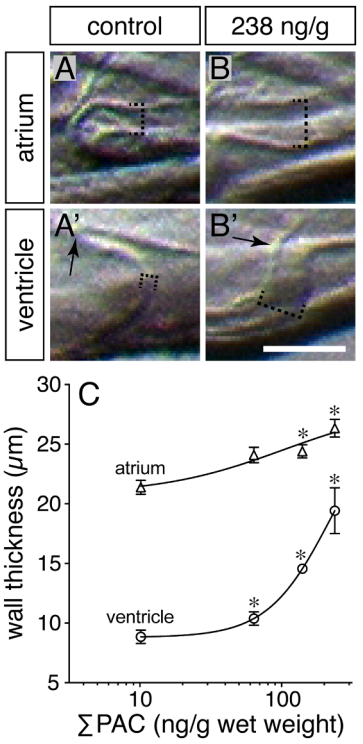

Fig. 3. Dose-dependent increase in atrial and ventricular wall thickness at hatch. Representative high magnification views of the ventral atrial wall (A, B) and posterior ventricular wall (A', B') were taken from video frames at end diastole for both chambers. (A, A') control, (B, B') 238 ng/g dose. Dotted black brackets indicate region of thickness measurements. Arrows (A', B') indicates position of the atrioventricular junction for the ventricle. (C) Thickness of atrial and ventricular walls (μm) quantified for 10 larvae from each of 4 replicate exposures (mean ± s.e.m., N = 4). Asterisks indicate groups that are statistically different from control (α = 0.05) by ANOVA and Dunnett post-hoc test. Scale bar (B') is 50 μm.

intracellular aryl hydrocarbon receptor. Levels of *cyp1a* mRNA induction were quantified in embryos throughout exposure at 6, 8 and 10 dpf, and at 14 dpf after four days of subsequent development and hatching in clean water. While the time course of *cyp1a* expression is detailed further below in the context of cardiac gene expression (Fig. 7A), maximal expression was observed at 10 dpf, with 10 ± 2, 33 ± 5 and 55 ± 8 fold-change induction relative to controls, respectively, corresponding to the 64, 140, and 238 ng/g doses. Notably, by 2 dph (4 days post-exposure), *cyp1a* levels declined to control levels across all doses (Fig. 7A).

3.3. Gross body morphology and incidence of edema

Oil exposure had no effect on hatch rates. After a hatching period of three days (15 dpf), mean hatch rates for control, 64, 140, and 238 ng/g doses were 83.5 ± 2.8, 88.1 ± 3.1, 90.0 ± 4.0, and 82.0 ± 7.6%, respectively (ANOVA p = 0.5). As observed previously across many species, trace oil exposures at the lower end of the concentration-response relationship yielded hatched larvae that appeared overtly normal, aside from mild-moderate pericardial edema (Fig. 1). A few larvae from the 238 ng/g dose showed mild dorsal curvature (Fig. 1D), but this was not frequent enough to quantify. As expected, newly hatched larvae displayed dose-dependent pericardial edema, with an EC_{50} of 244 ng/g ∑PAC (Fig. 1E). Despite the apparent shorter length of randomly selected oil-exposed larvae (e.g., Fig. 1B, C), there was no significant effect of exposure on the mass of embryos at exposure day 10 or newly hatched yolk-sac larvae (14 dpf), as determined by dry weight (Fig. 1F). At the first-feeding stage, after the absorption of yolk, there was a trend (p = 0.09) of reduced size in larvae from oil exposed groups (Fig. 1F, white bars), although high mortality in the 238 ng/g dose groups precluded sampling for dry weights.

3.4. Cardiac function and shape in yolk sac and first-feeding larvae

Similar to other marine species, the herring heart at late embryonic stages (e.g., 10 dpf) has a predominantly lateral orientation, with the opening of the atrium (sinus venosus) on the left side of the embryo and the ventricle to the right and slight anterior of the atrium (Fig. 2A). By the early yolk sac larval stage, the heart has migrated such that both chambers are aligned along the midline, with the atrium superior to the ventricle. The ventricle then begins to extend beneath the atrium posteriorly as an outgrowth or "ballooning" of the outer curvature (Fig. 2B). Oil exposure led to a dose-dependent decrease in ventricular ballooning measured at 14 dpf, or hatching day 2, four days post-exposure in clean seawater (Figs. 2C – E; 4A). Ventricular ballooning was highly sensitive to oil exposure, with significant reduction occurring at the 64 ng/g dose treatment and an IC_{50} of ∑PAC 87 ng/g (Fig. 4A). Ventricular ballooning continued in feeding stage larvae (20 dpf or 8 days post-hatch; dph), with posterior growth in controls extending past the cleithrum (Fig. S3A, C). In larva exposed to the 238 ng/g dose, ventricular ballooning had initiated by this stage, but in contrast to controls, had not yet extended to reach the cleithrum (Fig. S3B, D).

Delayed ventricular ballooning also correlated with an increase in the thickness of cardiac jelly, the clear extracellular matrix that lies between the endocardium and myocardium in the embryonic heart. At 14 dpf/1 dph, this was particularly evident in the posterior ventricle

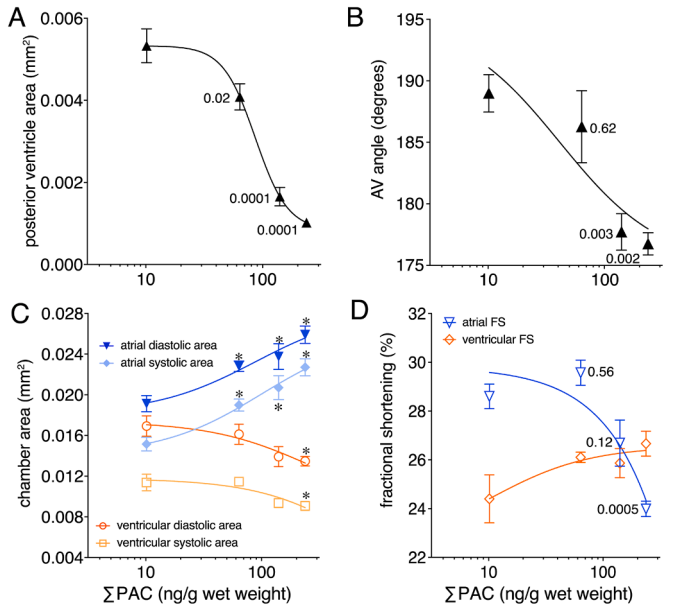

Fig. 4. Quantification of dose-dependent effects of oil exposure on cardiac morphology and function at hatch. All data are mean ± s.e.m. (N = 4) from at least 23 larvae from each of 4 replicate exposures for each dose at 1 dph, plotted against internal ∑PAC dose with non-linear regression models as described in the Materials and Methods section. Significance compared to control after ANOVA and Dunnett's post-hoc test is indicated by p values (A, B, D) or asterisks (C). (A) Area of the posterior ventricle (mm^2). (B) Atrioventricular (AV) angle (degrees). (C) Chamber areas (mm^2) for atrium at end diastole (blue triangles) and end systole (light blue diamonds), and ventricle at end diastole (orange circles) and end systole (light orange squares). (D) Contractility measured as fractional shortening for the atrium (blue triangles) and ventricle (orange diamonds).

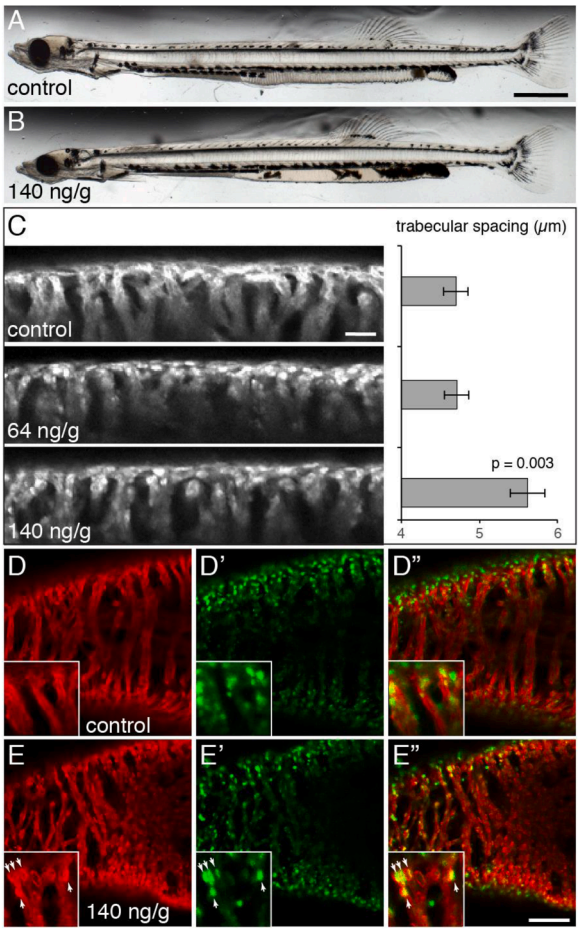

Fig. 5. Abnormal trabeculation in larvae surviving to 67 dpf. (A, B) Representative live larvae at 67 dpf from control (A) and ∑PAC 140 ng/g dose groups (B). (C) Confocal images of cortical and trabecular cardiomyocytes labeled with anti-myosin heavy chain antibody, with control at top, ∑PAC 64 ng/g dose in the middle and 140 ng/g dose at bottom. Images were collected from the center of the ventral wall of the ventricle, with the ventral cortical layer at top and trabeculae extending downward to the interior of the ventricle. Quantification of trabecular spacing immediately near the cortical layer is shown plotted to the right of the representative images. Data are mean ± s.e.m. of 13-14 trabecular spaces in each of 5 or 4 individual larvae for control and each exposed dose, respectively. ANOVA was significant for effect of exposure (p = 0.0025) with the 140 ng/g dose different from control by Dunnett's post-hoc test (p = 0.003). (D, E) Cardiomyocyte myosin heavy chain distribution (D, E; red) relative to nuclei (D', E'; green) in confocal images taken from the ventral aspect of the ventricle for control (D-D") and ∑PAC 140 ng/g dose (E-E"). Merged images shown in (D", E"). Inset in each shows higher magnification view of individual cells from the same image; arrows indicate co-localization of nuclei with spheroid myosin heavy chain immunofluorescence. Scale bars are 2 mm (A), 10 μm (C) and 50 μm (E").

(Fig. 3). In control yolk sac larvae, the atrial wall is much thicker than the ventricular wall (e.g., 21.4 ± 0.6 μm vs. 8.8 ±0.6 μm, respectively), largely due to more abundant cardiac jelly in the former (Fig. 3A, A'). Oil exposure led to a dose-dependent increase in the thickness of both chamber walls, visible in larvae from the 238 ng/g dose as a marked increase in ventricular cardiac jelly (Fig. 3B, B'). The increase in cardiac jelly was significant at the 64 ng/g dose (p = 0.03) for the ventricle and at the 140 ng/g dose (p = 0.006) for the atrium, with ventricular and atrial EC_{50}s at 103 ng/g and 222 ng/g tissue ∑PACs, respectively (Fig. 3C). In addition, oil exposure was also associated with the appearance of a "cap" or cellular thickening of the posterior ventricular wall (Fig. S4A, B), which was dose-dependent and occurred in up to 14.2 ± 4.3% of newly hatched larvae from the 238 ng/g dose (Fig. S4C). Whole-mount labeling of hearts with anti-myosin heavy chain antibodies followed by confocal microscopy demonstrated that these cellular caps represented solid, disorganized clusters of cardiomyocytes (Fig. S4D – F).

Other morphological changes included an impact on looping of the cardiac chambers. The atrioventricular (AV) angle was decreased in oil-exposed larvae (Fig. 4B), indicating abnormal looping. This was significant at the 140 ng/g dose, with an IC_{50} across treatments of 41 ng/g. In addition, an increase in the area of the atrium (Fig. 4C; blue shades) paralleled the decreased ventricular area (Fig. 4C; orange shades). The effect on atrial size was as sensitive as the reduced ventricular ballooning – i.e., significant in response to the lowest treatment. Importantly, the relationship between oil exposure and heart chamber area appeared the same for both diastolic (relaxed) and systolic (contracted) states. When the total area of the ventricle was measured, the effect was not as profound as on only the posterior ballooning portion (Fig. 4C; orange shades; compare to Fig. 4A), with only the highest dose significantly different than control. Finally, measurement of fractional shortening (Fig. 4D) showed a dose-dependent decrease in atrial contractility, but no effect on ventricular contractility. In contrast, there was no significant dose-dependent effect on heart rate at this stage, with rates for control, 64, 140, and 238 ng/g doses at 103 ± 5, 102 ± 6, 106 ± 4 and 100 ± 6 beats/min, respectively (ANOVA p = 0.9).

3.5. *Defective ventricular trabeculation in late larvae*

At 67 dpf there were ~200 surviving larvae in the control group, ~300 each for the 64 ng/g and 140 ng/g doses, and 62 for the 238 ng/g dose. Fish were approaching metamorphosis and appeared grossly indistinguishable by treatment (Fig. 5A, B). Cardiac structure was examined in subsamples of the 64 ng/g and 140 ng/g dose groups, but

Table 3.
Anatomical measurements in 125 dpf Pacific herring juveniles.

Measure	Control (N = 9)	∑PAC 64 ng/g (N = 18)	P value
length (mm)	27.4 ± 1.6	27.9 ± 0.8	0.76
wet weight (g)	0.079 ± 0.021	0.089 ± 0.011	0.63
K	0.32 ± 0.02	0.39 ± 0.02	0.03
ventricle lateral area (mm^2)	0.81 ± 0.08	0.91 ± 0.08	0.4
ventricle ventral area (mm^2)	0.99 ± 0.10	1.04 ± 0.05	0.6
ventricle lateral aspect ratio	2.17 ± 0.05	1.91 ± 0.04	0.0002
ventricle ventral aspect ratio	1.86 ± 0.07	1.76 ± 0.03	0.15

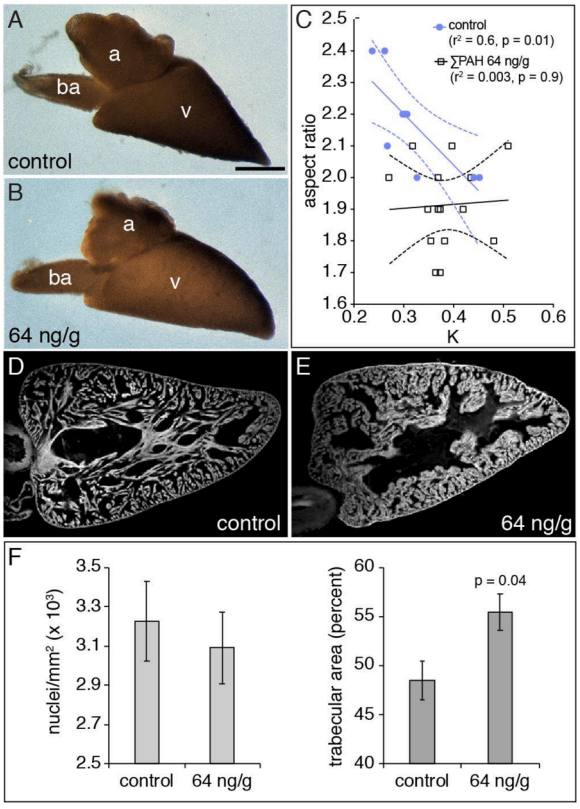

Fig. 6. Altered ventricular shape and hypertrophy of trabeculae in early juveniles at 125 dpf. Lateral views of freshly-dissected hearts from representative control (A) and 64 ng/g dose group (B). Anterior is to the left, dorsal at top. Ventricle, *v*; atrium, *a*; bulbus arteriosus, *ba*. Scale bar is 0.5 mm (A). (C) Linear regression model relating aspect ratio to condition factor K at 125 dpf in controls (N = 9; blue circles) and the 64 ng/g dose group (N = 15; black squares). Representative images of myosin heavy chain immunofluorescence in histological sections from a subset of 125 dpf hearts from control (D) and 64 ng/g dose group (E). Total cellularity (F, left plot) was quantified by counting DAPI-stained nuclei and normalizing to total pixel area occupied by myosin heavy chain labeling, while trabecular hypertrophy (F, right plot) was quantified as the percentage of pixels from myosin heavy chain labeling relative to total pixel area contained by the ventricle perimeter. Data represent mean ± s.e.m. of measurements from 2 to 3 replicate sections from each of 6 control hearts and 7 hearts from the 64 ng/g dose group. One-way nested ANOVA was significant for effect of treatment ($p = 0.04$) but not replicate ($p = 0.14$); post-hoc t-test showed a significant difference between control and exposed ($p = 0.04$).

not in the 238 ng/g dose group due to low numbers. To assess internal anatomy, hearts were whole-mount labeled with anti-myosin heavy chain antibody and imaged by confocal microscopy. At this stage, the ventricles still consisted of an outer, single layer of cortical cardiomyocytes with distinct, regularly spaced trabeculae (early bands of spongy myocardium) circumferentially arranged around the anterior-posterior axis and extending between the dorsal and ventral walls. Spacing between trabecular bases that extended from the cortical layer averaged 4.7 ± 0.2 μm in controls (Fig. 5C, top). While the trabecular spacing was unchanged for herring larvae in the 64 ng/g dose group (Fig. 5C, middle, also 4.7 ± 0.2 μm), there was a significant increase in the spacing between trabeculae at the 140 ng/g dose, at 5.6 ± 0.3 μm ($p = 0.003$; Fig. 5C, bottom). Unaltered trabecular spacing in the lowest dose group notwithstanding, all oil-exposed fish (5/5 fish examined for each dose) showed a distinctive change in the distribution of myosin heavy chain labeling, with the 64 ng/g and 140 ng/g treatments both showing highly irregular spherical or ovoid aggregations, as opposed to the more linear, fibrillar arrangements in controls (Fig. 5C). Labeling of nuclei with DAPI suggested that these spheroid/ovoid aggregates may represent individual cardiomyocytes with a rounder rather than elongated form (Fig. 5D, E). These abnormal forms were found not just near the cortical layer, but were present throughout the entire extent of the trabeculae (Fig. 5D, E).

3.6. Trabecular hypertrophy in early juveniles

At 125 dpf, the only surviving herring belonged to the control and 64 ng/g dose groups. Although there were no significant differences in length or mass (wet weight) between these two groups, the condition factor (K, a measure of length-weight proportionality) of the oil-exposed juveniles was 18% higher (0.32 vs. 0.39; Table 3). Dimensions of the ventricle were measured in ventral and lateral images collected after fixation, across the control and low oil groups, and gross heart anatomy was superficially very similar (Fig. 6A, B). Moreover, there were no significant differences in either the lateral or ventral areas of the ventricle (Table 23). However, while there was no significant difference in the ventral aspect ratio, the lateral aspect ratio was reduced from 2.17 ± 0.05 in controls to 1.91 ± 0.04 in the low dose group ($p = 0.0002$; Table 23). A relationship between ventricular shape, K, and swimming performance has been described for juvenile salmonids (Claireaux et al., 2005), with fish with higher K having rounder hearts and slower critical swimming speed. Similarly, in control herring at 125 dpf, there was a strong relationship between increasing K and decreased aspect ratio (rounder hearts) (Fig. 6C, circles; $r^2 = 0.6$, $p = 0.01$). However, in fish from the 64 ng/g dose group, there was no relationship between K and ventricular aspect ratio (Fig. 6C, squares.)

Trabecular structure was assessed in histological sections of the same hearts. Sections of control hearts at 125 dpf labeled with anti-myosin heavy chain generally showed an internal spongy myocardium consisting of a finely ordered meshwork of trabeculae, interspaced with prominent lumina of roughly equal area (Fig. 6D). In contrast, hearts from the 64 ng/g dose group showed denser, more irregular trabeculae with less pronounced luminal spaces between them (Fig. 6E). To determine if this represented a hypertrophic response to crude oil, we quantified the area occupied by trabecular cardiomyocytes by measuring pixels from anti-myosin heavy chain immunofluorescence, and assessed cellularity by counting nuclei stained with DAPI (Fig. 6F). Importantly, aggregate nuclei enumeration is a potentially indeterminate indicator of myocyte-specific toxicity as it is not possible to distinguish among nuclei in cardiomyocytes, endothelial cells, fibroblasts, erythrocytes or other cell types present in the ventricle. Nevertheless, normalizing the total count of nuclei to the area occupied by anti-myosin heavy chain labeling showed a trend of lower density for the exposed fish. While this was not statistically significant, this is suggestive of larger cardiomyocyte size in the oil exposed group. On the other hand, the total area occupied by trabecular myosin heavy chain labeling in the 64 ng/g dose group was increased significantly by 7% (55.4 ± 1.9% vs. 48.5 ± 2.0%; $p = 0.04$). This indicates, conversely, that the luminal space available for ventricular filling was reduced from approximately 51.5% to 44.6% in oil-exposed fish.

Table 4.
Target gene expression levels in heart vs. skeletal muscle of juvenile Pacific herring.

	Heart:skeletal muscle mean relative expression (N = 3)
myl7	469,744 ± 198,257
nkx2.5	70,468 ± 30,091
nrg2	61 ± 25
ryr2	24 ± 11
atp2a2	7 ± 1
notch1	6 ± 2
nac2	1.3 ± 0.1
myh7	0.2 ± 0.1
h*begfa*	0.2 ± 0.1

3.7. Changes in the expression of genes involved in cardiac Ca^{2+} handling, contractility, ventricular specification and trabeculation

We examined the transcription of four types of genes premised on the known effects of oil exposure on cardiac gene expression in mahi mahi (Coryphaena hippurus) (Edmunds et al., 2015; Xu et al., 2016) and Atlantic haddock (Sørhus et al., 2017; Sørhus et al., 2016b), as well as previous studies of normal trabeculation in zebrafish (Rasouli and Stainier, 2017; Samsa et al., 2016). This included intracellular Ca^{2+} handling (atp2a2, encoding SERCA2; nac2, encoding NCX2; and ryr2, encoding the ryanodine receptor 2 isoform), cardiac contractility (myl7/cmlc2, encoding the cardiac myosin light chain regulatory subunit, and myh7, encoding ventricular myosin heavy chain), the primary ventricular cardiomyocyte determination factor nkx2.5, and genes identified in zebrafish that function in trabeculation (notch1, nrg2, encoding neuregulin2, and hbegfa, encoding heparin-binding EGF-like growth factor). The absence of a sequenced Pacific herring genome hindered the verification of gene identity. To characterize these genes further, we compared expression levels in cardiac ventricle relative to skeletal muscle isolated from cultured 1-yr old juvenile fish. Most target gene mRNAs showed a relative enrichment in ventricle (Table 4; based mean of 3 individuals). The putative myh7 gene was expressed at roughly equal levels in juvenile ventricle and skeletal muscle. While the mammalian myh7 ortholog is expressed in both cardiac ventricle and slow-twitch skeletal muscle fibers (Quiat et al., 2011), myosin heavy chain gene phylogeny and expression patterns in teleosts are extremely complicated relative to mammals (McGuigan et al., 2004). The expression of this herring myh7 ortholog at relatively high levels in juvenile swimming muscle thus does not preclude it as the primary ventricular myosin heavy chain gene. As HB-EGF has a broad tissue distribution (Raab and Klagsbrun, 1997), the hbegfa gene would not necessarily be expected to show cardiac-specific expression.

Gene expression was first measured in 6 dpf embryos, at the onset of eye pigmentation and a point at which the heart had a regular beat, and sequentially thereafter at 8 dpf, 10 dpf, and after hatch (14 dpf; Fig. 7). The time course of PAC exposure relative to cardiotoxic response was evident from the dynamic expression pattern for *cyp1a* (Fig. 7A). Induction of *cyp1a* mRNA in response to oil was dose-dependent at 6 dpf, with expression peaking at 10 dpf (when internal tissue PACs were measured), and falling to baseline after transfer to clean water and hatch. Importantly, *cyp1a* induction was already at levels of 10- to nearly 30-fold within six days of oiled gravel column effluent exposure, indicating considerable PAC uptake. Of the three genes encoding Ca^{2+}-handling proteins, only *atp2a2* was significantly affected, transiently down-regulated ~2-fold at 6 dpf (Fig. 7B), with no significant effect on either *nac2* (Fig. 7C) or *ryr2* (Fig. 7D). Genes regulating contractility were significantly affected, with *myl7* showing a consistent trend of down-regulation, with a significant ~3-fold reduction at 8 dpf and at hatch (Fig. 7E). Similarly, *myh7* showed an overall trend of down-regulation with a significant dose-dependent effect at 8 dpf, with almost 5-fold reduction at the 238 ng/g dose (Fig. 7F). Notably, *nkx2.5* was significantly downregulated in both the 140 ng/g and 238 ng/g doses at hatch (Fig. 7G), coinciding with the small ventricle phenotype. For genes potentially involved in trabeculation, there was no significant effect on *notch1* mRNA abundance (Fig. 7H). However, there was a significant ~2-fold up-regulation of *nrg2* at 10 dpf and hatch in the 238 ng/g dose group (Fig. 7I), and a significant dose-dependent down-regulation of *hbegfa* at 6 and 8 dpf (Fig. 7J), with ~3-fold reduction in the 238 ng/g dose group. Detailed expression data are provided in Table S1.

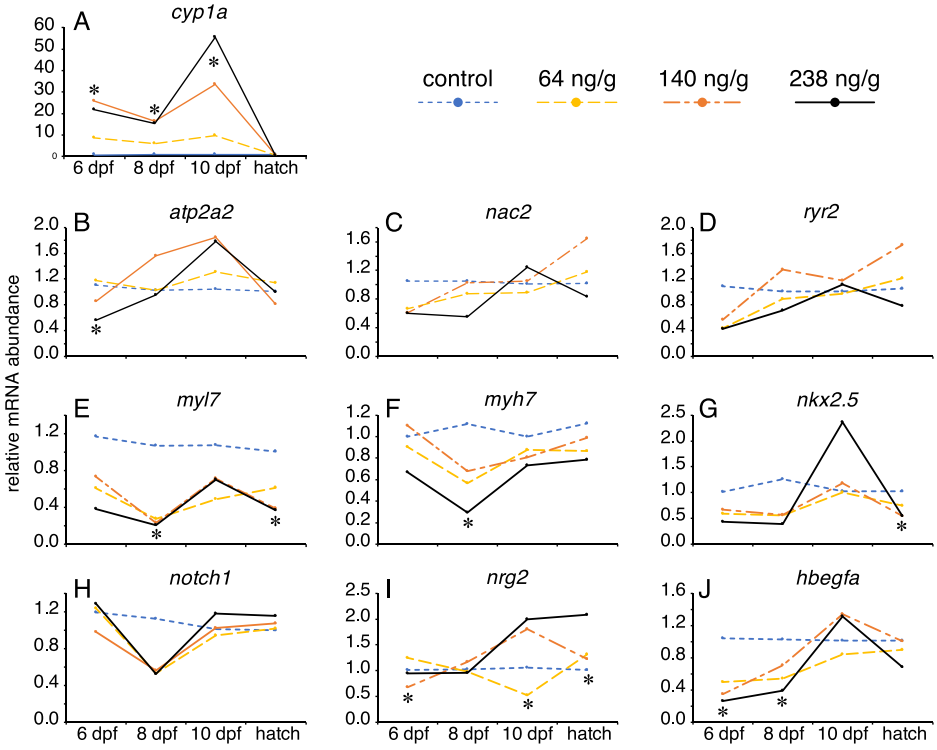

Fig. 7. Quantification of expression levels of genes functioning in cardiac Ca^{2+} handling, contractility, ventricular specification and trabeculation. As a reference for the exposure time course and PAC toxicokinetics, expression of *cyp1a* is shown in (A). Expression is shown for four time points; three during embryonic exposure (6 dpf, 8 dpf, 10 dpf) and one 3 days after exposure in yolk sac larvae (hatch). Dosing levels are color-coded, control (blue), 64 ng/g (yellow), 140 ng/g (orange) and 238 ng/g (black) tissue ∑PAC. For each gene, lines are plotted for each dose between each time point to highlight general trends. Data represent mean (N = 4) fold-change relative to controls normalized to the geometric mean of three reference genes (see Materials and methods). For simplicity, error bars are omitted, but complete set of raw data and variability are provided in Table S1. One-way ANOVAs were performed separately for each gene and each time point. If the ANOVA showed a $p \leq 0.05$ for effect of treatment, Dunnett's post-hoc test was performed to identify statistically different dose groups. Asterisks indicate groups that were statistically different from control ($p \leq 0.05$). (B) *atp2a2*; (C) *nac2*; (D) *ryr2*; (E) *myl7*; (F) *myh7*; (G) *nkx2.5*; (H) *notch1*; (I) *nrg2*; (J) *hbegfa*.

4. Discussion

The edematous syndrome that follows crude oil exposure in fish embryos results from heart failure. Studies that examined cardiac function closely in exposed embryos or larvae show a variety of defects relating to either contractility or rate/rhythm or both (Incardona, 2017; Incardona and Scholz, 2016). These whole-heart functional defects were recently linked to direct effects of PAC-rich mixtures or individual PACs on single-cell cardiomyocyte action potential generation, excitation-contraction coupling, and contractility (Brette et al., 2014; Brette et al., 2017; Vehniäinen et al., 2019). In our previous studies with Pacific herring embryos, we showed that exposure to the same Alaskan crude oil used here resulted in a pronounced slowing of the heart rate (bradycardia) and reduced contractility well before hatch at 7 dpf with tissue ∑PAC concentrations of 620 ng/g (Incardona et al., 2009), about 2.5-times higher than the high dose achieved here. The data presented here now clearly link those earlier functional defects to adverse effects on later morphogenetic maturation of the cardiac ventricle, at even lower doses, and in the absence of other visible extra-cardiac morphological phenotypes. In newly hatched larvae (14 dpf), ventricular ballooning was delayed in a manner highly dose-dependent on tissue PACs, as was the concomitant reduction in ventricular wall cardiac jelly. Despite a recovery in ballooning (by 20 dpf), subsequent trabeculation was dose-dependently disrupted in late larvae, along with a possible abnormal increase in cardiomyocyte proliferation (67 dpf). At the lowest dose tested, ∑PAC 64 ng/g wet weight, this led to hypertrophic changes within spongy myocardium in early juveniles (125 dpf). These findings directly link early impairment of embryonic cardiac function (contractility and fluid flow) from crude oil exposure to subsequent disruption of the co-dependent, downstream processes of ventricular ballooning and trabeculation in larvae and early juveniles. In turn, these defects in late steps of cardiac morphogenesis set the stage for much later pathological remodeling (hypertrophy) and reduced cardiorespiratory performance, as previously documented for older juvenile herring and pink salmon (Gardner et al., 2019; Incardona et al., 2015) or adult zebrafish (Hicken et al., 2011).

In virtually every species examined, a hallmark of acute oil cardiotoxicity to embryos is reduced contractility of one or both cardiac chambers (e.g., (Edmunds et al., 2015; Incardona et al., 2013; Morris et al., 2018; Sørhus et al., 2016b). This reduction in contractility is consistent with the rapid, direct effects of either select individual tricyclic compounds (e.g., phenanthrene) or a dissolved chemical mixture from whole oil on intracellular Ca^{2+} cycling in cardiomyocytes (Brette et al., 2014; Brette et al., 2017). In the present study *cyp1a* levels returned to baseline between the end of exposure (10 dpf) and hatching (14 dpf). This indicates that PACs were depurated by the time the ventricular morphological phenotype was initially observed. Thus, a transient oil-induced disruption of intracellular Ca^{2+} handling subsequently disrupted ballooning and trabecular morphogenesis.

Importantly, the observed dose-response relationships for morphological effects on the heart were very robust down to low ∑PAC concentrations, specifically ~ 1 μg/L in water and 64 ng/g in tissues. Based on an average molecular weight of ~200 g/mol for most petrogenic PACs, the latter represents a tissue concentration of ~320 nmol/kg. This is 1,000 to 10,000-fold lower than the tissue residue concentrations that have been ascribed to so-called "narcotic" or "baseline" toxicity in response to acute or chronic exposures (e.g., 2 – 8 mmol/kg and 0.2 – 0.8 mmol/kg, respectively; McCarty and Mackay, 1993). Instead, these tissue concentrations are consistent with specific receptor interactions, as supported by the cellular studies (Brette et al., 2014; Brette et al., 2017). For comparison, the Na^+/K^+-ATPase inhibitor digoxin affects cardiac contractility (positively) at concentrations of 200 nmol/kg in myocardial tissue (Steiness and Valentin, 1976). Therefore, in contrast to an adverse outcome framework premised on non-specific (or unspecified) toxicological processes, the consideration of tissue PACs in the context of cardiac function and heart morphogenesis is considerably more robust in terms of environmentally realistic exposures, defined mechanisms of action, the extrapolation of injury across biological scales, and the role of conserved evolutionary processes (e.g., calcium cycling in vertebrate cardiomyocytes) as determinants of individual-based toxic response. Despite remaining complexities surrounding the potency of dissolved petrogenic mixtures relative to single PAC compounds, our findings support the use of tissue PAC chemistry as an environmental indicator of likely toxicity to fish embryos and later life stages.

In the context of elucidating specific mechanisms underlying the injury phenotypes observed here, relevant aspects of cardiac morphogenesis have been detailed at the organ, cellular, and molecular levels in zebrafish. In particular, recent advances include a series of studies elucidating the mechanisms of ventricular ballooning and trabeculation (Sidhwani and Yelon, 2019). All fish hearts begin as a simple linear tube, which subsequently loops (folds and twists) at the AV junction to bring the atrial and ventricular chambers into an adjacent arrangement. At this point, the dimensions of the two chambers are similar, and the chamber walls consist of a single layer of cardiomyocytes. Subsequently, the ventricle initiates a rapid posterior expansion, ballooning, that involves both rearrangement and reorientation of existing cardiomyocytes and addition of new cardiomyocytes within the wall through proliferation. As ballooning progresses, trabeculation begins, as cardiomyocytes from the wall project inward, delaminate and proliferate, thus forming the underlying architecture of the spongy myocardium (Gupta and Poss, 2012).

In zebrafish, which develop more rapidly than herring (2 days to hatch vs. 12), ballooning commences from the outer curvature of the ventricle nearly concomitantly with looping. These initial steps of ventricular shaping and ballooning are driven by corresponding changes in the shape of individual ventricular cardiomyocytes (Auman et al., 2007), and changes in the orientation of neighboring cardiomyocytes within the outer curvature wall (Merks et al., 2018). Changes in cardiomyocyte shape are dependent on fluid flow, and both cell shape and fluid flow are dependent on actomyosin function, and by inference, intracellular Ca^{2+}. When either the coordinated contractions of the entire ventricle or blood flow therein are reduced by disruption of sarcomeric actomyosin function, ventricular cardiomyocytes fail to elongate properly (Auman et al., 2007). At the same time, the function of non-muscle cytoskeletal actomyosin controls cardiomyocyte shape changes through the planar cell polarity (PCP) signaling pathway, driving rearrangements of neighboring cardiomyocytes during ballooning (Merks et al., 2018).

PCP signaling is mediated by non-canonical Wnt ligands acting to control the orientation of cells with respect to one another and within larger fields of cells (Yingzi and Marek, 2015). This control of cellular orientation and cell-cell associations occurs by a process involving both cell adhesion and non-muscle myosin activity, as regulated by intracellular Ca^{2+} via calcium-dependent adhesion molecules (cadherins; Hale and Strutt, 2015) and the Ca^{2+}-dependent activation of non-muscle myosin (Somlyo and Somlyo, 2003). In zebrafish, PCP-mediated ventricular ballooning involves Wnt11 (Merks et al., 2018), a signaling protein that also regulates the conductance of Ca^{2+} through L-type calcium channels during the parallel developmental coordination of electrical coupling among ventricular cardiomyocytes (Panakova et al., 2010).

The ballooning process is thus directly dependent on intracellular Ca^{2+} in at least two distinct ways, whole chamber contractility driven by sarcomeric actomyosin and PCP-mediated cellular rearrangements driven by non-muscle actomyosin. The disruptive action of crude oil exposure on intracellular Ca^{2+} fluxes from both internal stores (the sarcoplasmic reticulum, SR) and the extracellular electrochemical gradient (via L-type calcium channels) would thus be expected to impinge directly on the aforementioned morphogenetic processes that drive ventricular ballooning. Moreover, these morphogenetic events would be further impaired, albeit indirectly, through reductions in both fluid forces and whole chamber contractility in response to crude oil

exposure. The observed recovery of ballooning over time is consistent with the depuration of PACs and consequent restoration of intracellular Ca^{2+} cycling and ventricular contractility. However, our current findings show that this delay in the normal timing of ventricular outgrowth has a cascading effect on subsequent trabeculation.

In zebrafish, looping and the initiation of ballooning occur between ~ 36 through 48 hours post-fertilization (hpf) (Glickman and Yelon, 2002; Staudt and Stainier, 2012), the developmental stage also roughly equivalent to hatching in Pacific herring. Trabeculation begins in larval zebrafish the next day (~ 60 hpf), and as described above for looping and ballooning, is also dependent on both ventricular contractility and fluid forces derived from blood flow (Peshkovsky et al., 2011; Staudt et al., 2014). Cardiomyocytes residing in the original, singular outer layer of the ventricle wall extend protrusions toward the interior, then leave the outer layer, migrating and proliferating as the trabeculae mature and project across the chamber. This process requires Notch1, which signals to the endocardium to produce Neuregulin2a and activate the epidermal growth factor (EGF) receptor family member Erbb2/4 in cardiomyocytes (Jimenez-Amilburu et al., 2016; Peshkovsky et al., 2011; Rasouli and Stainier, 2017; Samsa et al., 2015). In addition, several other EGF-like ligands are expressed during trabeculation, including *hbegfa* (Samsa et al., 2016). The spacing of trabeculae is determined in part by the migration and insertion of neural crest-derived cardiomyocytes into the initial ventricular wall, which subsequently express the Notch ligand Jag2b and signal to adjacent cells (Abdul-Wajid et al., 2018). Cardiac contraction and blood flow induce *notch1* expression in endocardial cells (Samsa et al., 2015), and ventricular cardiomyocytes respond to Notch signaling only after the normal degradation of the cardiac jelly that lies between the endocardial cells and cardiomyocytes (Del Monte-Nieto et al., 2018; Rasouli and Stainier, 2017). Furthermore, Notch signaling in ventricular cardiomyocytes is activated by chamber contraction not long after establishment of the regular heartbeat (~ 28 hpf in zebrafish) (Samsa et al., 2015). Thus, a transient oil-induced impact on cardiac contractility at the midpoint of cardiogenesis, as in the exposures here, could also disrupt trabeculation in the post-hatch ventricle by reducing or delaying Notch signaling. Consistent with this, the ventricular cardiac jelly layer did not degrade in oil-exposed herring larvae, and there was a corresponding accumulation of disorganized ventricular cardiomyocyte aggregations ("caps") at hatch. Therefore, the abnormal persistence of visible cardiac jelly is likely a novel and predictive endpoint for subsequent defects in trabeculation.

Embryonic oil exposure led to two separate and concentration-dependent effects on trabeculation in herring larvae. Specifically, the medium (140 ng/g) exposure increased the initial spacing of trabeculae and produced abnormal rounded aggregations of myosin heavy chain immunofluorescence. While the low treatment (64 ng/g) only affected myosin distribution, these fish survived and yet showed an increased trabecular density (hypertrophy) later on. The co-localization of the myosin heavy chain aggregates with nuclei suggests that these may represent proliferative cardiomyocytes. As cardiomyocytes divide during trabeculation in zebrafish, they become rounder, disassemble sarcomeres, and lose striated myofibrils before mitosis. A minimal pool of sarcomeres remains intact only at the rounded cell periphery, then myofibrils reassemble fully after division when subsequent daughter cells elongate (Uribe et al., 2018). The spherical forms observed here with myosin heavy chain antibody were likely recently divided (or dividing) cardiomyocytes, suggesting that transient embryonic crude oil toxicity induces an early (and basal) hyperproliferative response during larval trabeculation. Later determinants of trabeculation in zebrafish or other species are not yet known. However, our findings here for 67 dpf fish suggest that cardiomyocyte proliferation continues throughout the extent of the trabeculae in the maturing heart. Although we were unable to quantify individual cardiomyocyte density, the hypertrophy of the ventricle at 125 dpf is likely attributable to a relative increase in cell number and size. This would be consistent with previous observations of ventricular hypercellularity in oil-exposed pink salmon (Incardona et al., 2015), as well as an important recent discovery in zebrafish showing that loss of normal Notch1-mediated trabecular spacing in embryos causes pathological hypertrophy and reduced swimming performance in surviving adults (Abdul-Wajid et al., 2018). We therefore recommend that future studies of delayed oil toxicity in fish focus on pharmacological and biophysical-based disruptions of the genetic pathways that underpin trabeculation in the larval and juvenile heart.

The modification of the internal structure of the spongy myocardium provides an additional, novel clue into the longstanding puzzle of why zebrafish (Hicken et al., 2011) and herring and pink salmon (Incardona et al., 2015) exposed to trace concentrations of crude oil relatively briefly during embryogenesis nevertheless show a reduction in cardio-respiratory performance that persists into much later stages of life – i.e., after many months of normal feeding and growth in clean water. In adult fish, organ-level gross morphometry initially implicated a rounder ventricle shape in reduced cardiac output and swimming performance found naturally (Claireaux et al., 2005), or as a consequence of embryonic oil exposure (Hicken et al., 2011). While the structure of the compact myocardium was not assessed in oil-exposed fully mature, adult zebrafish (11 months post-exposure) (Hicken et al., 2011), embryonic oil exposure in pink salmon led to a thinning of the juvenile compact myocardium (8- to 10-months post-exposure), and both pink salmon and herring juveniles showed elongated rather than rounded ventricles (i.e., increased aspect ratio) (Incardona et al., 2015). The determinants of ventricular shape in juvenile herring or salmon are unclear, nor is the relationship between ventricular shape and cardiac output. However, luminal volume and the density of trabeculation are likely to more consistently influence cardiac output at earlier juvenile stages when the compact myocardium consists of only a single layer of cardiomyocytes and has not begun to proliferate. Notably, at the stages studied here (125 dpf, ~ 4 months post-exposure), the compact myocardium had not yet begun to proliferate and was still only a single layer of cardiomyocytes, but we still observed a similar elongation of the ventricle as observed in 10-month old oil-exposed fish with a multicellular compact myocardium (Incardona et al., 2015). Intriguingly, controls showed an inverse relationship between condition factor and ventricular aspect ratio, while oil-exposed fish showed no relationship. Therefore, embryonic oil exposure overrides the normal factors controlling ventricular shape in juveniles. It is possible that the hypertrophic response we observed here in the early juvenile spongy myocardium leads to elongation of the ventricle, which left unabated, could continue on to produce a terminally rounded ventricle in fully adult, near-senescent fish. Additional studies should focus on how this crude oil injury phenotype ultimately impacts individual survival.

From the perspective of assessing losses of culturally, ecologically, and commercially important fishes, it would be advantageous to identify molecular markers for normal and pathophysiological heart development in species that spawn in clean and contaminated environments, respectively. Such biological indicators (or molecular initiating events) could meet a wide array of resource management needs, including field-based determinations of injury in habitats degraded by PACs originating from oil spills, urban stormwater runoff, and legacy sediment pollution. To this end, we focused here on quantification of gene expression using real-time PCR. QPCR is suitable for the sample sizes typical of fish early life history stages, rapidly adaptable across multiple species, and offers a platform that is potentially adaptable to remote sensing in future field studies. Nevertheless, there remain a few key challenges to this approach. The first is the need to accurately measure tissue-specific changes in gene expression against a backdrop of mRNA extracted from whole animals. This signal-to-noise problem is particularly important for oil-responsive genes that are expressed at a relatively low level but have an outsized influence on embryolarval development (Sørhus et al., 2016a; Sørhus et al., 2017). Some of these genes are known to be cardiac-specific or expressed only in the heart at the embryonic stages studied here, while others have broader expression

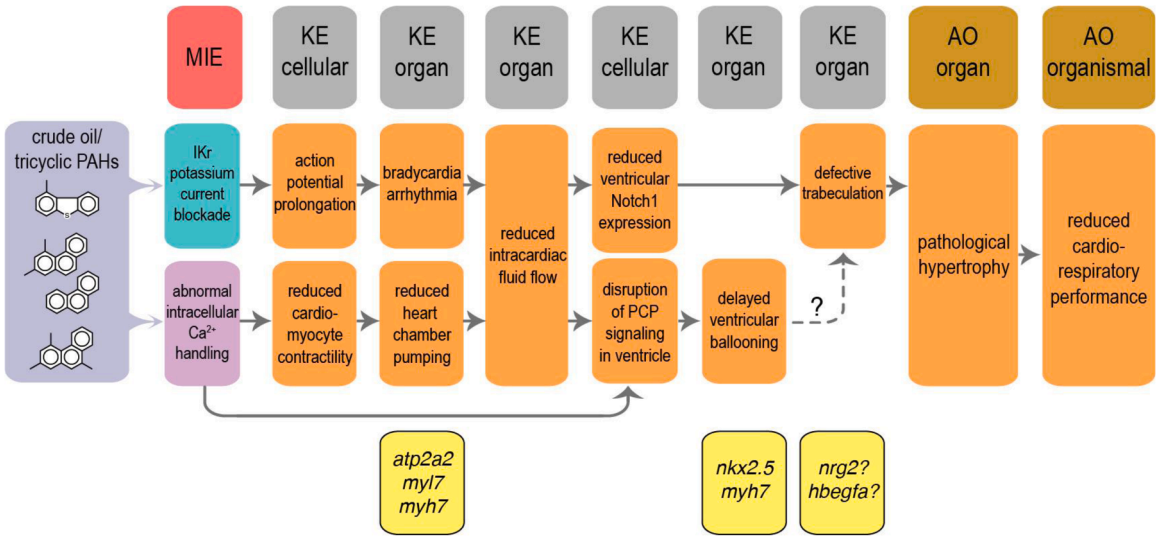

Fig. 8.. Model summarizing the adverse outcome pathway for low-level crude oil toxicity during fish embryonic development. *MIE*, molecular initiating event; *KE*, key event; *AO*, adverse outcome. Gene expression markers identified in this study are indicated in the boxes along the far right.

patterns in multiple embryonic structures. The second is the challenge of gene annotation and isoform identification in non-model species, with or without a sequenced genome. Target genes can be selected using a hypothesis-driven approach based on anchoring to a well-defined injury phenotype (Edmunds et al., 2015; Sørhus et al., 2016b) or, as we have done here, chosen based on the results of transcriptome sequencing in other species (Sørhus et al., 2017; Xu et al., 2016). A final challenge relating to this approach is that many of these target genes, especially those expressed only in the developing heart, are very low abundance transcripts. The variability inherent in measuring low abundance genes creates a demand for higher statistical power, which itself often conflicts with what is logistically feasible for sampling strategies with fish embryos and larvae.

Recognizing the above limitations, we assessed the expression of genes encoding the major Ca^{2+}-handling proteins in cardiomyocytes. These included the SR Ca^{2+} release channel (ryanodine receptor isoform 2; *ryr2*), the SR Ca^{2+} uptake pump (SERCA2; *atp2a2*), and the plasma membrane Na^{+}/Ca^{2+} exchanger (NCX1; *nac1/2/4*). In embryos and early larvae of other species, one or more of these genes were down-regulated in response to controlled crude oil exposures (Sørhus et al., 2017; Sørhus et al., 2016b; Xu et al., 2016). This includes an Atlantic haddock contig originally identified as *nac1* but most closely related to a herring *nac2* isoform (as determined via a BLAST search) that was expressed in both juvenile heart and skeletal muscle. While neither *nac2* nor *ryr* expression was altered significantly in the experiments described, *atp2a2* was transiently down-regulated very early during exposure and at roughly the same developmental stage as previously reported for Atlantic haddock (Sørhus et al., 2017).

By convention, distinct morphogenetic phenotypes serve to anchor the interpretation of changing gene expression patterns. For example, severe heart malformations in haddock at hatching (prior to ventricular ballooning) were preceded by the strong up-regulation of the Ca^{2+}-regulated cardiac morphogen bone morphogenetic protein 10 (*bmp10*) (Sørhus et al., 2017; Sørhus et al., 2016b) and subsequent upregulation of *nkx2.5*, a downstream, positive target of *bmp10*. However, in mahi mahi (Edmunds et al., 2015) and Pacific herring (present study) hatching with milder malformations, *nkx2.5* as well as *myl7* and *myh7* were down-regulated. The down-regulation of these three genes is therefore consistent with (or indicative of) the more nuanced crude oil cardiotoxicity phenotypes of reduced contractility (during exposure) and reduced size of the ventricle (after exposure) at hatch. Among the known roles for *nkx2.5* in vertebrate heart development, the gene in zebrafish specifies the binary fate of cardiomyocyte precursors into atrium- and ventricle-specific subtypes, with reduced *nkx2.5* function leading to a smaller ventricle (Targoff et al., 2013). While we did not quantify the number of atrial cardiomyocytes as a potential mechanism, the enlarged atria and the smaller ventricles observed here may be a consequence of an oil-induced down-regulation of *nkx2.5*.

Finally, we examined the expression of *notch1, nrg2*, and *hbegfa*, candidate genes with known or potential roles in zebrafish ventricular trabeculation. In zebrafish, all three are expressed in multiple embryonic tissues external to the heart, creating a challenge for interpreting gene expression levels from whole-embryo total mRNA. Of these, for example, *notch1* has the broadest expression, with high levels in the developing central nervous system (Thisse and Thisse, 2005). Read-count data in Atlantic haddock embryos provides the ability to link whole-embryo mRNA levels to expression patterns characterized by in situ hybridization (Sørhus et al., 2016a; Sørhus et al., 2017). In this case, genes that show cardiac-specific expression by in situ hybridization had read counts that averaged about 90, while those with broader expression, for example throughout the somites or neural tube, had read counts of ~ 2000 – 9000. In Atlantic haddock embryos, which are similar in size to Pacific herring, read counts for mRNAs of *notch1, nrg2* and *hbegf* were in the range of 2000 – 12,000, ~ 100, and 20 – 50, respectively. Thus, the oil-induced effects on expression of *nrg2* and *hbegfa* are likely to reflect changes linked to the ventricular phenotype, while changes in cardiac *notch1* expression might not be resolved against such a large pool of extracardiac mRNA. Because of this broad expression, a negative result with *notch1* is equivocal, and the role of cardiac *notch1* expression in abnormal heart form and function in response to oil exposure will require further study. The effects of oil on the other putative trabeculation genes in herring embryos were stage-specific, including both early down-regulation (*hbegfa*) and late up-regulation (*nrg2*), the latter possibly as a consequence of over-compensation as tissue PAC concentrations declined and cardiac function was restored. Future confirmation of gene expression at a cellular level via in situ hybridization will further elucidate mechanisms of dysregulated ventricular trabeculation. Nevertheless, these findings represent an important step in the development of new biomarkers for delayed and persistent cardiotoxicity in response to low-level oil exposure.

In summary, these results expand our understanding of how acute, transient, and sublethal crude oil toxicity in fish embryos produces a latent pathological remodeling of the post-hatching heart, thereby reducing cardiorespiratory performance in surviving juveniles. The tissue doses measured here, when normalized to lipids, overlap with previous studies showing impacts on ventricular structure and function

delayed even further in time in both Pacific herring and pink salmon (Incardona et al., 2015). This is consistent with an adverse outcome pathway for crude oil toxicity in fish that extends from the disruption of excitation-contraction coupling within embryonic cardiomyocytes to defective trabeculation to pathological hypertrophy at the scale of the maturing organ (Fig. 8). We have identified potential molecular indicators for key events in this pathway, in the form of genes functioning in cardiac contractility (*atp2a2, myl7, myh7*), ventricular cardiomyocyte specification (*nkx2.5*) and trabeculation (*nrg2, hbegfa*). Promisingly, for example, the down-regulation of *myl7* and *myh7* genes is consistently associated with contractility defects across several fish species. Finally, the delayed heart malformations observed here would likely be sufficient to explain the reduced marine survival of pink salmon in previous mark and recapture studies (Heintz, 2007; Heintz et al., 2000). It is notable, however, that these cardiac defects were evident in herring under controlled aquaculture conditions. In natural habitats, the confluence of crude oil cardiotoxicity and other environmental co-stressors such as thermal variation, predation, and pathogen exposures would likely further reduce individual survival and, by extension, recruitment to populations that support humans and aquatic ecosystems.

Author contributions

Conceptualization: JPI, TLL, JC, KAP, SEA, NLS; Study Investigation: JPI, TLL, BLL, JC, KAP, CAL, MBH, GH, DTB; Data curation: JPI, TLL, BLL, JC, KAP, CAL, MBH, GH, DTB, GMY; Writing - original draft: JPI, TLL, JC, KAP; Manuscript Writing - review & editing: JPI, SEA, GMY, NLS; Project administration: JPI, GMY, NLS; Funding acquisition: JPI, SEA, NLS.

Declaration of Competing Interest

The authors declare that they have no known competing financial interests or personal relationships that could have appeared to influence the work reported in this paper.

Acknowledgments

We thank Mary Arkoosh for use of wet and dry lab space at the Newport facility; Joe Dietrich for assistance with designing and building the exposure system and preparing growth tanks; Paul Iseri for small boat operations and herring fishing; Jana Labenia, David Baldwin, Jessica Lundin, and Julann Spromberg for assistance with exposures and sampling; and Paul Hershberger and Jake Gregg for providing juvenile herring for the comparative qPCR in heart and swimming muscle samples. We thank Julann Spromberg for her critical review of the manuscript. Funding was provided in part by the NOAA National Ocean Service, Office of Response and Restoration, Assessment and Restoration Division.

Supplementary materials

Supplementary material associated with this article can be found, in the online version, at doi:10.1016/j.aquatox.2021.105810.

References

Abdul-Wajid, S., Demarest, B.L., Yost, H.J., 2018. Loss of embryonic neural crest derived cardiomyocytes causes adult onset hypertrophic cardiomyopathy in zebrafish. Nat. Commun. 9, 4603.

Adeyemo, O.K., Kroll, K.J., Denslow, N.D., 2015. Developmental abnormalities and differential expression of genes induced in oil and dispersant exposed Menidia beryllina embryos. Aquat. Toxicol. 168, 60–71.

Andrés-Delgado, L., Mercader, N., 2016. Interplay between cardiac function and heart development. Biochim. Biophys. Acta 1863, 1707–1716.

Arnaout, R., Ferrer, T., Huisken, J., Spitzer, K., Stainier, D.Y., Tristani-Firouzi, M., Chi, N. C., 2007. Zebrafish model for human long QT syndrome. Proc. Natl. Acad. Sci. U. S. A. 104, 11316–11321.

Auman, H.J., Coleman, H., Riley, H.E., Olale, F., Tsai, H.J., Yelon, D., 2007. Functional modulation of cardiac form through regionally confined cell shape changes. PLoS Biol. 5, e53.

Berdougo, E., Coleman, H., Lee, D.H., Stainier, D.Y., Yelon, D., 2003. Mutation of *weak atrium/atrial myosin heavy chain* disrupts atrial function and influences ventricular morphogenesis in zebrafish. Development 130, 6121–6129.

Brette, F., Machado, B., Cros, C., Incardona, J.P., Scholz, N.L., Block, B.A., 2014. Crude oil impairs cardiac excitation-contraction coupling in fish. Science 343, 772–776.

Brette, F., Shiels, H.A., Galli, G.L.J., Cros, C., Incardona, J.P., Scholz, N.L., Block, B.A., 2017. A novel cardiotoxic mechanism for a pervasive global pollutant. Sci. Rep. 7, 41476.

Carls, M.G., Rice, S.D., Hose, J.E., 1999. Sensitivity of fish embryos to weathered crude oil: part I. Low-level exposure during incubation causes malformations, genetic damage, and mortality in larval Pacific herring (*Clupea pallasi*). Environ. Toxicol. Chem. 18, 481–493.

Claireaux, G., McKenzie, D.J., Genge, A.G., Chatelier, A., Aubin, J., Farrell, A.P., 2005. Linking swimming performance, cardiac pumping ability and cardiac anatomy in rainbow trout. J. Exp. Biol. 208, 1775–1784.

Del Monte-Nieto, G., Ramialison, M., Adam, A.A.S., Wu, B., Aharonov, A., D'Uva, G., Bourke, L.M., Pitulescu, M.E., Chen, H., de la Pompa, J.L., Shou, W., Adams, R.H., Harten, S.K., Tzahor, E., Zhou, B., Harvey, R.P., 2018. Control of cardiac jelly dynamics by NOTCH1 and NRG1 defines the building plan for trabeculation. Nature 557, 439–445.

Dietrich, A.C., Lombardo, V.A., Veerkamp, J., Priller, F., Abdelilah-Seyfried, S., 2014. Blood flow and Bmp signaling control endocardial chamber morphogenesis. Dev. Cell 30, 367–377.

Ebert, A.M., Hume, G.L., Warren, K.S., Cook, N.P., Burns, C.G., Mohideen, M.A., Siegal, G., Yelon, D., Fishman, M.C., Garrity, D.M., 2005. Calcium extrusion is critical for cardiac morphogenesis and rhythm in embryonic zebrafish hearts. Proc. Natl. Acad. Sci. U. S. A. 102, 17705–17710.

Edmunds, R.C., Gill, J.A., Baldwin, D.H., Linbo, T.L., French, B.L., Brown, T.L., Esbaugh, A.J., Mager, E.M., Stieglitz, J.D., Hoenig, R., Benetti, D.D., Grosell, M., Scholz, N.L., Incardona, J.P., 2015. Corresponding morphological and molecular indicators of crude oil toxicity to the developing hearts of mahi mahi. Sci. Rep. 5, 17326.

Esbaugh, A.J., Mager, E.M., Stieglitz, J.D., Hoenig, R., Linbo, T.L., Lay, C., Forth, H., Brown, T.L., French, B.L., Scholz, N.L., Incardona, J.P., Morris, J.M., Benetti, D.D., Grosell, M., 2016. The effects of weathering and chemical dispersion on Deepwater Horizon crude oil toxicity to mahi-mahi (*Coryphaena hippurus*) early life stages. Sci. Total Environ. 543, 644–651.

Gardner, L.D., Peck, K.A., Goetz, G.W., Linbo, T.L., Cameron, J., Scholz, N.L., Block, B.A., Incardona, J.P., 2019. Cardiac remodeling in response to embryonic crude oil exposure involves unconventional NKX family members and innate immunity genes. J. Exp. Biol. 222, jeb205567.

Glickman, N.S., Yelon, D., 2002. Cardiac development in zebrafish: coordination of form and function. Semin. Cell Dev. Biol. 13, 507–513.

Griffin, F.J., Pillai, M.C., Vines, C.A., Kaaria, J., Hibbard-Robbins, T., Yanagimachi, R., Cherr, G.N., 1998. Effects of salinity on sperm motility, fertilization, and development in the Pacific herring, Clupea pallasi. Biol. Bull. 194, 25–35.

Gupta, V., Poss, K.D., 2012. Clonally dominant cardiomyocytes direct heart morphogenesis. Nature 484, 479–484.

Hale, R., Strutt, D., 2015. Conservation of planar polarity pathway function across the animal kingdom. Annu. Rev. Genet. 49, 529–551.

Hatlen, K., Sloan, C.A., Burrows, D.G., Collier, T.K., Scholz, N.L., Incardona, J.P., 2010. Natural sunlight and residual fuel oils are an acutely lethal combination for fish embryos. Aquat. Toxicol. 99, 56–64.

Heintz, R.A., 2007. Chronic exposure to polynuclear aromatic hydrocarbons in natal habitats leads to decreased equilibrium size, growth, and stability of pink salmon populations. Integr. Environ. Assess. Manag. 3, 351–363.

Heintz, R.A., Rice, S.D., Wertheimer, A.C., Bradshaw, R.F., Thrower, F.P., Joyce, J.E., Short, J.W., 2000. Delayed effects on growth and marine survival of pink salmon Oncorhynchus gorbuscha after exposure to crude oil during embryonic development. Mar. Ecol. Prog. Ser. 208, 205–216.

Hicken, C.E., Linbo, T.L., Baldwin, D.H., Willis, M.L., Myers, M.S., Holland, L., Larsen, M., Stekoll, M.S., Rice, G.S., Collier, T.K., Scholz, N.L., Incardona, J.P., 2011. Sub-lethal exposure to crude oil during embryonic development alters cardiac morphology and reduces aerobic capacity in adult fish. Proc. Natl. Acad. Sci. U. S. A. 108, 7086–7090.

Incardona, J.P., 2017. Molecular mechanisms of crude oil developmental toxicity in fish. Arch. Environ. Contam. Toxicol. 73, 19–32.

Incardona, J.P., Carls, M.G., Day, H.L., Sloan, C.A., Bolton, J.L., Collier, T.K., Scholz, N. L., 2009. Cardiac arrhythmia is the primary response of embryonic Pacific herring (Clupea pallasi) exposed to crude oil during weathering. Environ. Sci. Technol. 43, 201–207.

Incardona, J.P., Carls, M.G., Holland, L., Linbo, T.L., Baldwin, D.H., Myers, M.S., Peck, K. A., Rice, S.D., Scholz, N.L., 2015. Very low embryonic crude oil exposures cause lasting cardiac defects in salmon and herring. Sci. Rep. 5, 13499.

Incardona, J.P., Carls, M.G., Teraoka, H., Sloan, C.A., Collier, T.K., Scholz, N.L., 2005. Aryl hydrocarbon receptor-independent toxicity of weathered crude oil during fish development. Environ. Health Perspect. 113, 1755–1762.

Incardona, J.P., Collier, T.K., Scholz, N.L., 2004. Defects in cardiac function precede morphological abnormalities in fish embryos exposed to polycyclic aromatic hydrocarbons. Toxicol. Appl. Pharmacol. 196, 191–205.

Incardona, J.P., Gardner, L.D., Linbo, T.L., Brown, T.L., Esbaugh, A.J., Mager, E.M., Stieglitz, J.D., French, B.L., Labenia, J.S., Laetz, C.A., Tagal, M., Sloan, C.A., Elizur, A., Benetti, D.D., Grosell, M., Block, B.A., Scholz, N.L., 2014. Deepwater horizon crude oil impacts the developing hearts of large predatory pelagic fish. Proc. Natl. Acad. Sci. U. S. A. 111.

Incardona, J.P., Scholz, N.L., 2016. The influence of heart developmental anatomy on cardiotoxicity-based adverse outcome pathways in fish. Aquat. Toxicol. 177, 515–525.

Incardona, J.P., Scholz, N.L., 2018. Case study: the 2010 Deepwater Horizon oil spill, in: Burggren, W., Dubansky, B. (Eds.), Development, Physiology, and Environment: A Synthesis. Springer, London.

Incardona, J.P., Swarts, T.L., Edmunds, R.C., Linbo, T.L., Edmunds, R.C., Aquilina-Beck, A., Sloan, C.A., Gardner, L.D., Block, B.A., Scholz, N.L., 2013. Exxon Valdez to deepwater horizon: comparable toxicity of both crude oils to fish early life stages. Aquat. Toxicol. 142-143, 303–316.

Incardona, J.P., Vines, C.A., Anulacion, B.F., Baldwin, D.H., Day, H.L., French, B.L., Labenia, J.S., Linbo, T.L., Myers, M.S., Olson, O.P., Sloan, C.A., Sol, S., Griffin, F.J., Menard, K., Morgan, S.G., West, J.E., Collier, T.K., Ylitalo, G.M., Cherr, G.N., Scholz, N.L., 2012a. Unexpectedly high mortality in Pacific herring embryos exposed to the 2007 Cosco Busan oil spill in San Francisco Bay. Proc. Natl. Acad. Sci. U. S. A. 109, E51–E58.

Incardona, J.P., Vines, C.A., Linbo, T.L., Myers, M.S., Sloan, C.A., Anulacion, B.F., Boyd, D., Collier, T.K., Morgan, S., Cherr, G.N., Scholz, N.L., 2012b. Potent phototoxicity of marine bunker oil to translucent herring embryos after prolonged weathering. PLoS One 7, e30116.

Jimenez-Amilburu, V., Rasouli, S.J., Staudt, D.W., Nakajima, H., Chiba, A., Mochizuki, N., Stainier, D.Y.R., 2016. In vivo visualization of Cardiomyocyte apicobasal polarity reveals epithelial to Mesenchymal-like transition during cardiac trabeculation. Cell Rep. 17, 2687–2699.

Jung, J.-H., Hicken, C.E., Boyd, D., Anulacion, B.F., Carls, M.G., Shim, W.J., Incardona, J. P., 2013. Geologically distinct crude oils cause a common cardiotoxicity syndrome in developing zebrafish. Chemosphere 91, 1146–1155.

Jung, J.H., Kim, M., Yim, U.H., Ha, S.Y., Shim, W.J., Chae, Y.S., Kim, H., Incardona, J.P., Linbo, T.L., Kwon, J.H., 2015. Differential toxicokinetics determines the sensitivity of two marine embryonic fish exposed to Iranian heavy crude oil. Environ. Sci. Technol. 49, 13639–13648.

Jung, J.H., Lee, E.H., Choi, K.M., Yim, U.H., Ha, S.Y., An, J.G., Kim, M., 2017. Developmental toxicity in flounder embryos exposed to crude oils derived from different geographical regions. Comp. Biochem. Physiol. C-Pharmacol. Toxicol. Endocrinol. 196, 19–26.

Khursigara, A.J., Perrichon, P., Martinez Bautista, N., Burggren, W.W., Esbaugh, A.J., 2017. Cardiac function and survival are affected by crude oil in larval red drum, Sciaenops ocellatus. Sci. Total Environ. 579, 797–804.

Laurel, B.J., Copeman, L.A., Iseri, P., Spencer, M.L., Hutchinson, G., Nordtug, T., Donald, C.E., Meier, S., Allan, S.E., Boyd, D.T., Ylitalo, G.M., Cameron, J.R., French, B.L., Linbo, T.L., Scholz, N.L., Incardona, J.P., 2019. Embryonic crude oil exposure impairs growth and lipid allocation in a keystone Arctic forage fish. iScience in press.

Li, X., Ding, G., Xiong, Y., Ma, X., Fan, Y., Xiong, D., 2018. Toxicity of water-accommodated fractions (WAF), chemically enhanced WAF (CEWAF) of Oman crude oil and dispersant to early-life stages of zebrafish (Danio rerio). Bull. Environ. Contam. Toxicol. 101, 314–319.

Linden, O., 1978. Biological effects of oil on early development of the Baltic herring *Clupea harengus membras*. Mar. Biol. 45, 273–283.

Ljubojevic, S., Bers, D.M., 2015. Nuclear calcium in cardiac myocytes. J. Cardiovasc. Pharmacol. 65, 211–217.

Madison, B.N., Hodson, P.V., Langlois, V.S., 2017. Cold Lake Blend diluted bitumen toxicity to the early development of Japanese medaka. Environ. Pollut. 225, 579–586.

Martinez Barrio, A., Lamichhaney, S., Fan, G.C., Rafati, N., Pettersson, M., Zhang, H., Dainat, J., Ekman, D., Höppner, M., Jern, P., Martin, M., Nystedt, B., Liu, X., Chen, W., Liang, X., Shi, C., Fu, Y., Ma, K.C., Zhan, X., Feng, C., Gustafson, U., Rubin, C.-J., Sällman Almén, M., Blass, M., Casini, M., Folkvord, A., Laikre, L., Ryman, N., Ming-Yuen Lee, S., Xu, X., Andersson, L., 2016. The genetic basis for ecological adaptation of the Atlantic herring revealed by genome sequencing. eLife 5, e12081.

Marty, G.D., Hose, J.E., McGurk, M.D., Brown, E.D., Hinton, D.E., 1997. Histopathology and cytogenetic evaluation of Pacific herring larvae exposed to petroleum hydrocarbons in the laboratory or in Prince William Sound, Alaska, after the Exxon Valdez oil spill. Can. J. Fish. Aquat. Sci. 54, 1846–1857.

McCarty, L.S., Mackay, D., 1993. Enhancing ecotoxicological modeling and assessment. Body residues and modes of toxic action. Environ. Sci. Technol. 27, 1718–1728.

McGuigan, K., Phillips, P.C., Postlethwait, J.H., 2004. Evolution of Sarcomeric myosin heavy chain genes: evidence from fish. Molec. Biol. Evol. 21, 1042–1056.

McKechnie, I., Lepofsky, D., Moss, M.L., Butler, V.L., Orchard, T.J., Coupland, G., Foster, F., Caldwell, M., Lertzman, K., 2014. Archaeological data provide alternative hypotheses on Pacific herring (Clupea pallasii) distribution, abundance, and variability. Proceed. Natl. Acad. Sci. 111, E807–E816.

Merks, A.M., Swinarski, M., Meyer, A.M., Müller, N.V., Özcan, I., Donat, S., Burger, A., Gilbert, S., Mosimann, C., Abdelilah-Seyfried, S., Panáková, D., 2018. Planar cell polarity signalling coordinates heart tube remodelling through tissue-scale polarisation of actomyosin activity. Nat. Commun. 9, 2161.

Miquerol, L., Kelly, R.G., 2013. Organogenesis of the vertebrate heart. Wiley Interdiscipl. Rev. 2, 17–29.

Morris, J., Gielazyn, M., Krasnec, M., Takeshita, R., Forth, H., Labenia, J.S., Linbo, T.L., French, B.L., Gill, J.A., Baldwin, D.H., Scholz, N.L., Incardona, J.P., 2018. Crude oil cardiotoxicity to red drum embryos is independent of oil dispersion energy. Chemosphere 213, 205–214.

Nolan, T., Hands, R.E., Bustin, S.A., 2006. Quantification of mRNA using real-time RT-PCR. Nat. Protoc. 1, 1559–1582.

Panakova, D., Werdich, A.A., Macrae, C.A., 2010. Wnt11 patterns a myocardial electrical gradient through regulation of the L-type Ca(2+) channel. Nature 466, 874–878.

Peshkovsky, C., Totong, R., Yelon, D., 2011. Dependence of cardiac trabeculation on neuregulin signaling and blood flow in zebrafish. Dev. Dyn. 240, 446–456.

Pollino, C.A., Holdway, D.A., 2002. Toxicity testing of crude oil and related compounds using early life stages of the crimson-spotted rainbowfish (*Melanotaenia fluviatilis*). Ecotox. Environ. Saf. 52, 180–189.

Quiat, D., Voelker, K.A., Pei, J., Grishin, N.V., Grange, R.W., Bassel-Duby, R., Olson, E.N., 2011. Concerted regulation of myofiber-specific gene expression and muscle performance by the transcriptional repressor Sox6. Proc. Natl. Acad. Sci. U. S. A. 108, 10196–10201.

Raab, G., Klagsbrun, M., 1997. Heparin-binding EGF-like growth factor. Biochim. Biophys. Acta 1333, F179–F199.

Raine, J.C., Turcotte, D., Tumber, V., Peru, K.M., Wang, Z., Yang, C., Headley, J.V., Parrott, J.L., 2017. The effect of oil sands tailings pond sediments on embryo-larval walleye (Sander vitreus). Environ. Pollut. 229, 798–809.

Rasouli, S.J., Stainier, D.Y.R., 2017. Regulation of cardiomyocyte behavior in zebrafish trabeculation by Neuregulin 2a signaling. Nat. Commun. 8, 15281.

Roberts, S.B., Hauser, L., Seeb, L.W., Seeb, J.E., 2012. Development of genomic resources for Pacific herring through targeted transcriptome pyrosequencing. PLOS ONE 7, e30908.

Rottbauer, W., Baker, K., Wo, Z.G., Mohideen, M.A., Cantiello, H.F., Fishman, M.C., 2001. Growth and function of the embryonic heart depend upon the cardiac-specific L-type calcium channel alpha1 subunit. Dev. Cell 1, 265–275.

Samsa, L.A., Givens, C., Tzima, E., Stainier, D.Y.R., Qian, L., Liu, J.D., 2015. Cardiac contraction activates endocardial Notch signaling to modulate chamber maturation in zebrafish. Development 142, 4080–4091.

Samsa, L.A., Ito, C.E., Brown, D.R., Qian, L., Liu, J., 2016. IgG-containing isoforms of Neuregulin-1 are dispensable for cardiac trabeculation in zebrafish. PLoS One 11, e0166734.

Schmittgen, T.D., Livak, K.J., 2008. Analyzing real-time PCR data by the comparative C (T) method. Nat. Protoc. 3, 1101-1111o1108.

Sidhwani, P., Yelon, D., 2019. Fluid forces shape the embryonic heart: insights from zebrafish. Curr. Top. Dev. Biol. 132, 395–416.

Sloan, C.A., Anulacion, B.F., Baugh, K.A., Bolton, J.L., Boyd, D., Boyer, R.H., Burrows, D. G., Herman, D.P., Pearce, R.W., Ylitalo, G.M., 2014. Northwest Fisheries Science Center's analyses of tissue, sediment, and water samples for organic contaminants by gas chromatography/mass spectrometry and analyses of tissue for lipid classes by thin layer chromatography/flame ionization detection NOAA Technical Memorandum, p. 61.

Somlyo, A.P., Somlyo, A.V., 2003. Ca2+ Sensitivity of smooth muscle and nonmuscle myosin II: modulated by G proteins, kinases, and myosin phosphatase. Physiol. Rev. 83, 1325–1358.

Sørhus, E., Incardona, J.P., Furmanek, T., Jentoft, S., Meier, S., Edvardsen, R.B., 2016a. Developmental transcriptomics in Atlantic haddock: illuminating pattern formation and organogenesis in non-model vertebrates. Dev. Biol. 411, 301–313.

Sørhus, E., Incardona, J.P., Furmanek, T., Scholz, N.L., Meier, S., Edvardsen, R.B., Jentoft, S., 2017. Novel adverse outcome pathways revealed by chemical genetics in a developing marine fish. eLife 6, e20707.

Sørhus, E., Incardona, J.P., Karlsen, Ø., Linbo, T.L., Sørensen, L., Nordtug, T., van der Meeren, T., Thorsen, A., Thorbjørnsen, M., Jentoft, S., Edvardsen, R.B., Meier, S., 2016b. Effects of crude oil on haddock reveal roles for intracellular calcium in craniofacial and cardiac development. Sci. Rep. 6, 31058.

Staudt, D., Stainier, D., 2012. Uncovering the molecular and cellular mechanisms of heart development using the zebrafish. Annu. Rev. Genet. 46, 397–418.

Staudt, D.W., Liu, J.D., Thorn, K.S., Stuurman, N., Liebling, M., Stainier, D.Y.R., 2014. High-resolution imaging of cardiomyocyte behavior reveals two distinct steps in ventricular trabeculation. Development 141, 585–593.

Steiness, E., Valentin, N., 1976. Myocardial digoxin uptake: dissociation between digitalis-induced inotropism and myocardial loss of potassium. Br. J. Pharmacol. 58, 183–188.

Targoff, K.L., Colombo, S., George, V., Schell, T., Kim, S.-H., Solnica-Krezel, L., Yelon, D., 2013. Nkx genes are essential for maintenance of ventricular identity. Development 140, 4203–4213.

Thisse, C., Thisse, B., 2005. High Throughput Expression Analysis of ZF-Models Consortium Clones. ZFIN Direct Data Submission.

Uhler, A.D., Stout, S.A., Douglas, G.S., 2007. Chemical heterogeneity in modern marine residual fuel oils, in: Wang, Z., Stout, S.A. (Eds.), Oil Spill Environmental Forensics. Academic Press, London, pp. 327-348.

Uribe, V., Ramadass, R., Dogra, D., Rasouli, S.J., Gunawan, F., Nakajima, H., Chiba, A., Reischauer, S., Mochizuki, N., Stainier, D.Y.R., 2018. In vivo analysis of cardiomyocyte proliferation during trabeculation. Development 145, dev164194.

Vehniäinen, E.R., Haverinen, J., Vornanen, M., 2019. Polycyclic aromatic hydrocarbons Phenanthrene and Retene modify the action potential via multiple ion currents in rainbow trout Oncorhynchus mykiss cardiac myocytes. Environ. Toxicol. Chem. 38, 2145–2153.

Wamhoff, B.R., Bowles, D.K., Owens, G.K., 2006. Excitation-transcription coupling in arterial smooth muscle. Circ. Res. 98, 868–878.

Wang, Z., Hollebone, B.P., Fingas, M., Fieldhouse, B., Sigouin, L., Landriault, M., Smith, P., Noonan, J., Thouin, G., Weaver, J.W., 2003. Characteristics of Spilled Oils, Fuels, and Petroleum Products: 1. Composition and Properties of Selected Oils. U.S. Environmental Protection Agency, Washington, D.C.

Xie, F.L., Xiao, P., Chen, D.L., Xu, L., Zhang, B.H., 2012. miRDeepFinder: a miRNA analysis tool for deep sequencing of plant small RNAs. Plant Mol. Biol. 80, 75–84.
Xu, E.G., Mager, E.M., Grosell, M., Pasparakis, C., Schlenker, L.S., Stieglitz, J.D., Benetti, D., Hazard, E.S., Courtney, S.M., Diamante, G., Freitas, J., Hardiman, G., Schlenk, D., 2016. Time- and oil-dependent transcriptomic and physiological responses to deepwater horizon oil in Mahi-Mahi (Coryphaena hippurus) embryos and larvae. Environ. Sci. Technol. 50, 7842–7851.
Yingzi, Y., Marek, M., 2015. Wnt-Frizzled/planar cell polarity signaling: cellular orientation by facing the wind (Wnt). Annu. Rev. Cell Dev. Biol. 31, 623–646.